

Double Modulation
- Optical Scanning and Mechanical Chopping -
in Atomic Absorption Spectrometry Using a Continuum Source

By

ROBERT COOPER ELSER

A DISSERTATION PRESENTED TO THE GRADUATE COUNCIL OF
THE UNIVERSITY OF FLORIDA IN PARTIAL
FULFILLMENT OF THE REQUIREMENTS FOR THE DEGREE OF
DOCTOR OF PHILOSOPHY

UNIVERSITY OF FLORIDA
1971



UNIVERSITY OF FLORIDA



3 1262 08552 4816

DEDICATION

The work contained in this dissertation represents the attainment of a goal which would have been exceedingly difficult without the love and encouragement of my wife, Kay. It is to her and to her understanding that I dedicate this dissertation.

ACKNOWLEDGMENTS

Any author has many debts to colleagues and teachers who have aided and guided him along the way. In this regard, I must express my gratitude to Dr. John Savory, who believed in me when it counted, to Drs. Eugene Sander, Gerhard Schmid and Roger Bates for their guidance as teachers and especially to Dr. James D. Winefordner for his direction and encouragement of my work. To Mr. Theodore Booher I owe a debt which can never be repaid, that of his friendship, encouragement and advice when it was needed most.

TABLE OF CONTENTS

	Page
ACKNOWLEDGMENTS	iii
LIST OF TABLES.	vi
LIST OF FIGURES	vii
KEY TO SYMBOLS.	ix
ABSTRACT:	xii
 Chapter	
I. INTRODUCTION.	1
II. THEORETICAL CONSIDERATIONS.	7
Mechanical Chopper Modulation.	7
Refractor Plate Modulation	9
Intensity Expressions.	14
Limits of Detection.	33
Signal-to-Noise Ratio.	37
III. EXPERIMENTAL SYSTEM AND PROCEDURES.	38
Description of System.	38
Source	38
Burner and Nebulizer	48
Monochromator and Optics	49
Electronic Components.	55
Solutions.	57
Experimental Procedure	58

Chapter	Page
IV. RESULTS AND DISCUSSION	60
Verification of Theory.	60
Analytical Curves and Limits of Detection	66
Conclusions	85
LIST OF REFERENCES	88
BIOGRAPHICAL SKETCH.	90

LIST OF TABLES

Table	Page
1. Breakdown of Intensity Expression $B_T(\lambda_c, t)$. .	22
2. Optical Components	41
3. Electrical Components.	43
4. Verification of Theory	61
5. Limits of Detection.	84

LIST OF FIGURES

Figure	Page
1a. Refraction of an axial beam incident to the refractor plate at an angle, α	11
1b. Refraction of a non-axial beam incident to the refractor plate at an angle, α	11
2. Schematic diagram of the optical system.	16
3a. First derivative of Ca resonance line profile at $4227 \overset{\circ}{\text{Å}}$ at a concentration of 25 ug ml^{-1}	29
3b. Second derivative of Ca resonance line profile at $4227 \overset{\circ}{\text{Å}}$ at a concentration of 25 ug ml^{-1}	29
4. Theoretical curve of growth for Ca at $4227 \overset{\circ}{\text{Å}}$ by first derivative analysis	32
5. Block diagram of experimental system	40
6. Relative spectral radiance of xenon arc.	46
7. Electrode holder for piezoelectric transducer.	51
8. Spectral modulation amplitude (slit image displacement) versus voltage supplied to the bimorph.	53
9. Circuit for chopper reference signal	54
10. First derivative signal intensity versus spectral modulation amplitude (slit image displacement) at constant spectral bandwidth of $0.40 \overset{\circ}{\text{Å}}$	63
11. Analytical curve for silver taken at $3200 \overset{\circ}{\text{Å}}$	68
12. Analytical curve for calcium taken at $4227 \overset{\circ}{\text{Å}}$	70
13. Analytical curve for cadmium taken at $2288 \overset{\circ}{\text{Å}}$	72
14. Analytical curve for chromium taken at $3579 \overset{\circ}{\text{Å}}$	74

Figure	Page
15. Analytical curve for copper taken at $3247 \overset{\circ}{\text{A}}$.	76
16. Analytical curve for iron taken at $3719 \overset{\circ}{\text{A}}$. .	78
17. Analytical curve for magnesium taken at $2852 \overset{\circ}{\text{A}}$	80
18. Analytical curve for nickel taken at $3414 \overset{\circ}{\text{A}}$.	82

KEY TO SYMBOLS

- a = Lateral displacement of refracted beam, Å.
- A = Atomic weight, amu.
- B = Factor accounting for noise contribution from dynodes, no units.
- $B_{\lambda_0}^0$ = Unmodulated source spectral radiance, watts $\text{cm}^{-2} \text{sr}^{-1} \text{nm}^{-1}$.
- $B_{\lambda_0}^c$ = Modulated source spectral radiance, watts $\text{cm}^{-2} \text{sr}^{-1} \text{nm}^{-1}$.
- $B_{\lambda_T}^c$ = Radiance transmitted through flame, watts $\text{cm}^{-2} \text{sr}^{-1} \text{nm}^{-1}$.
- $B_T(\lambda_c, t)$ = Modulated spectrum viewed by phototube, watts.
- c = Speed of light, cm sec^{-1} .
- C_m = Minimum detectable solution concentration, $\mu\text{g ml}^{-1}$.
- d = Lateral geometric displacement of refracted beam, mm.
- e = Electronic charge, 1.6×10^{-19} coulomb.
- E_i = Excitation energy of state i , ev.
- Δf = Frequency interval over which amplifier readout system responds, Hz.
- g_i = Statistical weight of state i .
- H = Monochromator slit height, cm.
- \bar{A}_{i_p} = rms noise signal due to the photodetector, amperes.
- J = Total angular momentum quantum number.
- k = Boltzmann constant, $8.64 \times 10^{-5} \text{ ev } ^\circ\text{K}^{-1}$.

- k_0^{in} = Peak atomic absorption coefficient for the minimum detectable concentration, cm^{-1} .
- k_0 = Atomic absorption coefficient at the absorption line center, cm^{-1} .
- \bar{k}_λ = Modified atomic absorption coefficient, cm^{-1} .
- l = Length of flame, cm.
- M = Multiplication (amplification)-factor of photodetector, no units.
- n = Total atomic concentration of species of interest, atom cm^{-3} .
- n_m = Total minimum atomic concentration of species of interest in flame, atom cm^{-3} .
- n_m^i = Minimum atomic concentration of species of interest in state i in flame, atom cm^{-3} .
- Q = Flow rate of unburned gases, $\text{cm}^3 \text{sec}^{-1}$.
- R_d = Reciprocal linear dispersion of monochromator, $\text{\AA} \text{mm}^{-1}$.
- R'_d = Reciprocal linear dispersion of monochromator, $\text{\AA} \text{cm}^{-1}$.
- R_L = Phototube load resistor, ohms.
- s = Spectral bandwidth of monochromator, \AA .
- $S(\lambda)$ = Slit function of the monochromator, no units.
- $S_{e_1+e_2}^1$ = First derivative signal, volt.
- $S_{e_1+e_2}^2$ = Second derivative signal, volt.
- T = Absolute temperature, $^\circ\text{K}$.
- T_f = Transmission factor of instrumental system of lenses, monochromator and flame.
- $T(\lambda)$ = Transmission of flame cell.

- t = Thickness of refractor plate, mm.
 W = Monochromator slit width, cm.
 $Z(T)$ = Electronic partition function, no units.
 α = Angle of beam incident to refractor plate, rad.
 α' = Angle of refracted beam within refractor plate, rad.
 β = Factor to account for incomplete atom formation and losses due to ionization, no units.
 γ = Phototube sensitivity factor, amp watt⁻¹.
 δ = Parallel displacement of refracted beam, mm.
 Δ = Apparent half-width of absorption line, Å.
 ϵ = Efficiency of nebulization and atomization processes.
 λ = Any wavelength, Å.
 λ_c = Wavelength at center of exit slit corresponding to grating setting, Å.
 λ_o = Wavelength at center of absorption line profile, Å.
 $\Delta\lambda_A$ = Half-width of absorption line, Å.
 $\frac{\pi e^2}{mc^2} = 2.65 \times 10^{-2} \text{ cm}^2 \text{ sec}^{-1}$.
 ρ = Coefficient to correct k_o .
 ϕ = Flow rate of solution into nebulizer, cm³ min⁻¹.
 Ω_M = Solid angle of radiation collected by the monochromator, sr.
 ω_1 = Frequency of source modulation, sec⁻¹.
 ω_2 = Frequency of wavelength modulation, sec⁻¹.

Abstract of Dissertation Presented to the Graduate Council
of the University of Florida in Partial Fulfillment of the
Requirements for the Degree of Doctor of Philosophy

DOUBLE MODULATION
- OPTICAL SCANNING AND MECHANICAL CHOPPING -
IN ATOMIC ABSORPTION SPECTROMETRY USING A CONTINUUM SOURCE

By

Robert Cooper Elser

June, 1971

Chairman: James Dudley Winefordner
Major Department: Chemistry

Atomic absorption spectrometry using a continuum source (AAC) presents several advantages distinct from atomic absorption using line sources. Among these are a saving in time of analysis, saving in cost of sources and the capability of non-resonance line absorption measurements. An instrumental system employing double modulation - mechanical chopping of source radiation and wavelength modulation of radiation transmitted by the absorption cell - offers advantages over normal AAC. Improvement in signal-to-noise ratios and decreased sensitivity to background as compared to normal AAC are the most important advantages. In this work, a doubly modulated system is described and the theory underlying its operation derived. It is shown that both first and second derivatives of the transmitted

spectrum can be obtained. The first derivative appears at a frequency equal to the sum or the difference of the two modulation frequencies, while the second derivative appears at the sum or the difference of the chopping frequency and twice the wavelength modulation frequency. Experiments are described which verify the validity of the theoretical expressions. Analytical curves and limits of detection are presented for the following eight elements: Ag, Ca, Cd, Cr, Cu, Fe, Mg and Ni.

CHAPTER I

INTRODUCTION

Atomic absorption spectrometry has proven its utility as a practical analytical tool in laboratories throughout the world over the past fifteen years since Walsh [1] introduced it in 1955. In his classic paper, he indicated that the measurement of the atomic absorption line profile of an element in a flame should provide a clue as to the atomic concentration in the flame. However, in order to resolve the spectral profile of an absorption line, monochromators having nearly unattainable resolving power would be required. Furthermore, the question of whether a continuum would have sufficient spectral energy in an interval of the size of an absorption line, that is 0.01 to 0.03 Å, to provide an acceptable signal-to-noise ratio led him to propose that measurement of the peak atomic absorption coefficient at the line center using a line source would provide similar quantitative information. Because an atomic line source concentrates most of its spectral output into the resonance lines characteristic of that element, it would provide sufficient energy in the

spectral interval of interest in addition to lowering the resolving power criterion for the monochromator to that of having the capability of merely isolating the spectral line of interest from any close lying lines. Because of these arguments, the development of atomic absorption instrumentation has excluded the use of continuum sources to a large extent. It is unfortunate that this has been the case since continuum sources offer several advantages over line sources. These have been enumerated by several authors [2,3,4,5,6] and include the requirement of having only one source instead of a source for each element (or small groups of elements) of interest; the saving of time in source alignment, and ease of background correction. In addition, McGee and Winefordner [2] and Fassel et al. [5] have shown that the limits of detection by atomic absorption using a continuum source approaches that using line sources for many elements. At low concentrations of absorber, however, the absorption line half-width becomes insignificant with respect to the spectral bandwidth of the monochromator and while the line may be discerned, the signal-to-noise ratio is low. It was thought that the weak signal due to the absorption line profile could be extracted from the noise and enhanced by using a derivative technique which has been employed successfully in other areas of spectroscopy.

The technique of derivative spectroscopy, that is, taking the derivative of the transmitted spectrum with respect to time or wavelength, was first introduced in 1955 by Giese and French [7]. They demonstrated its theoretical utility in resolving overlapping absorption bands having as much as 90 per cent overlap. Collier and Singleton [8] applied the technique to infrared absorption spectra by taking the second derivative of the spectrum electronically. However, as Bonfiglioli and Brovetto [9] and Perregaux and Ascarelli [10] point out, analog differentiation of the detector output results in treatment of the noise component contained in the signal as well as the information component. The frequency spectrum of the noise component differs from the frequency spectrum of the information component. Therefore, the noise in the derivative signal may become a greater proportion than in the original signal with the result that the signal-to-noise ratio of the derivative signal is lower than that of the original signal. Bonfiglioli and Brovetto developed the theory for a self-modulating derivative optical spectrometer [9] which employed a vibrating mirror to modulate the image of the spectrum. They showed, as will be derived in Chapter II, that by modulating the spectrum spatially and detecting at the appropriate frequency, the derivative of the transmitted spectrum may be obtained. In this manner, only the derivative of the desired

signal is obtained, with the noise component of the signal maintaining its relative proportion or even decreasing. In fact, noise arising from random fluctuations in phototube output proved to be the limiting noise in the derivative system. Since this type of photon noise has a constant spectral noise power over the entire frequency spectrum, its contribution to the signal will be identical for both modulated and unmodulated systems. Their system proved efficacious in the analysis of complex molecular absorption bands [11] of rare earth nitrates in aqueous solutions.

Various ingenious techniques have been employed in obtaining a modulated spectrum. Stauffer and Sakai [12] used a rotating mirror stepped along one diameter to modulate the spectrum image by a discrete amount. Balslev [13] modulated the exit slit of his monochromator by mechanically linking it to a loudspeaker vibrating at 175 Hz. The derivative spectrum obtained was used to study the influence of stress on the indirect optical absorption edge in silicon and germanium crystals. Williams and Hager [14] also employed an oscillating exit slit to study the second derivative absorption spectra of gaseous atmospheric pollutants. Perregaux and Ascarelli [10] studied the first derivative absorption spectrum of I_2 in an incandescent lamp using a glass refractor plate to modulate the spectrum. In their system, the plate was epoxied to a steel ribbon which

was oscillated by means of a piezoelectric bimorph. Shaklee and Rowe [15] used a fused silica refractor plate to modulate the reflectance spectra of InP and GaP at several temperatures. Snelleman et al. [16] modulated the emission spectra of elements in a flame using a quartz refractor plate and by operating in the second derivative mode were able to detect Ba in the presence of large amounts of Ca. The first application of derivative spectrometry to atomic absorption was by Snelleman [17] who used a mirror to scan the image of the dispersed spectrum across the exit slit of the monochromator. It was primarily his work which led to the development of the present system.

A continuum source and double modulation, that is, modulation of the radiation falling on the flame and emerging from it, was employed in this experimental system. A theory was developed to predict the response of the instrumentation to variation of experimental parameters. Several authors [9,13,14,15,18,19] have developed theoretical intensity expressions for derivative spectrometers. However, none have used their expressions as quantitative predictors of experimental signals. The derivation of theoretical expressions in this work closely parallels the derivations of Bonfiglioli and Brovotto [9] and Shaklee and Rowe [15]. The quantitative predictions of the theory were investigated and the system was used to construct analytical

curves and limits of detection for eight elements: Ag, Ca, Cd, Cr, Cu, Fe, Mg, and Ni.

CHAPTER II

THEORETICAL CONSIDERATIONS

Mechanical Chopper Modulation

In atomic absorption spectrophotometry, it is important to eliminate any signal arising in the absorption cell which is not due to absorption of source radiation. Since in most atomic absorption systems the absorption cell is a flame, there are three possible spurious sources of signal arising in the cell: emission due to flame gas combustion products; atomic emission and/or fluorescence of analyte atoms in the flame, and Rayleigh scattering of source radiation by small unevaporated solvent droplets or other small particles. Fortunately, in most cases, none of these has much effect upon the radiation passing through the flame. However, because atomic absorption signals are due to the attenuation of source radiation by absorbing species in the flame, any emission due to flame gas products or analyte atoms will decrease this attenuation and cause an apparent decrease in absorption which would be interpreted as a smaller concentration of absorbers in the absorption cell. Likewise, Rayleigh scattering of source radiation

would increase the attenuation of the radiation passing through the flame which would be interpreted as a higher concentration of absorbers in the flame than were actually there.

By modulating the source radiation and measuring the detector signal at the modulation frequency and with the correct phase relationship, emission from the flame cell can be rejected. The effect of Rayleigh scattering is eliminated by wavelength modulation. As a result of the source modulation, the signal due to absorbing species appears as an ac component, at the frequency of modulation, superimposed upon the dc signal due to flame cell emission. In practice, source modulation is usually accomplished by mechanical chopping using a motor driven disk having alternating transparent and opaque sectors which intersect the beam of radiation emanating from the source along the optical path of the system.

The modulated source radiation, if it is focussed on the chopper disk, is actually nearly square-wave modulated. However, in order to treat the system mathematically, it is convenient to assume the source radiation is sinusoidally modulated. In this case, the modulated source spectral radiance, $B_{\lambda_0}^c$ (watts centimeter⁻² steradian⁻¹ nanometer⁻¹), may be expressed as

$$B_{\lambda_0}^c = \frac{1}{2} B_{\lambda_0}^D (1 + \cos \omega_1 t) \quad (1)$$

where $B_{\lambda_0}^0$ is the unmodulated source spectral radiance (watts $\text{cm}^{-2}\text{sr}^{-1}\text{nm}^{-1}$) and ω_1 is the frequency of source modulation. In Equation (1) it is assumed that there are equally sized transparent and opaque sectors and therefore

$$B_{\lambda_{\text{AVG}}}^c = \frac{1}{2}B_{\lambda_0}^0 \quad (2)$$

where $B_{\lambda_{\text{AVG}}}^c$ is the average source spectral radiance incident upon the flame cell.

Refractor Plate Modulation

The wavelength modulation of the system is accomplished in this work by the use of an oscillating quartz plate. Because the index of refraction of the quartz plate is different from that of air, a beam of light incident on the plate will be refracted if its angle of incidence varies from 0° . The lateral displacement of the refracted beam may be expressed as

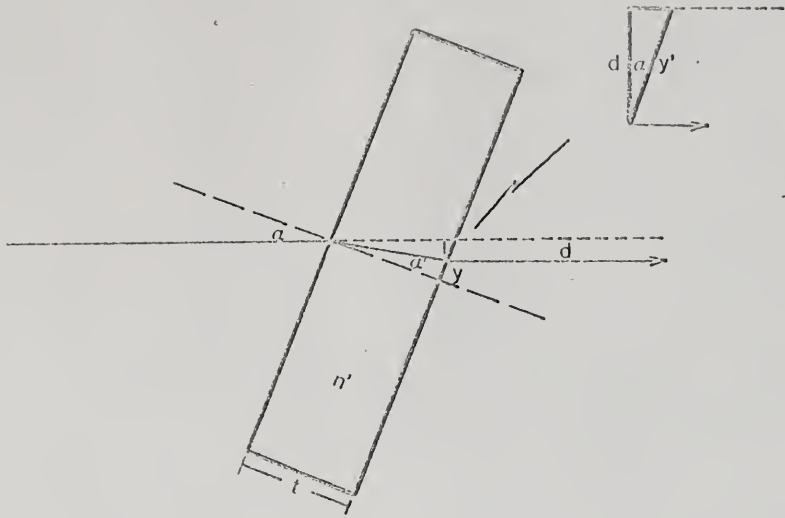
$$d = t \cdot \cos \alpha (\tan \alpha - \tan \alpha') \quad (3)$$

where d is the lateral displacement (mm), t is the plate thickness (mm), α is the angle of incidence and α' is the angle of refraction. It may be clearly seen from Figure 1a that the following relations hold

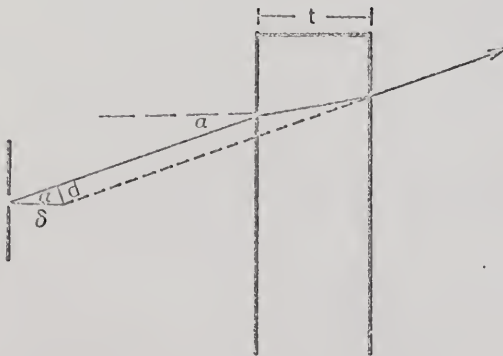
$$\cos \alpha = \frac{d}{Y'} \quad , \quad \tan \alpha = \frac{Y+Y'}{t} \quad , \quad \tan \alpha' = \frac{Y}{t} \quad (4)$$

Fig. 1a.--Refraction of an axial beam incident to
the refractor plate at an angle, α .

Fig. 1b.--Refraction of a non-axial beam incident
to the refractor plate at an angle, α .



a



b

By rearranging and substituting, one obtains Equation (3).

From Snell's law

$$n \tan \alpha = n' \tan \alpha' \quad (5)$$

where n and n' are the index of refraction of air and the plate, respectively. Substitution of Equation (5) into Equation (3) yields the exact expression for the lateral displacement

$$d = t \cdot \cos \alpha \left(\tan \alpha - \frac{n}{n'} \tan \alpha \right) \quad (6)$$

For very small angles $\cos \alpha$ is nearly unity and $\sin \alpha$ is approximately α . Considering n to be unity, the small angle approximation for the lateral displacement becomes

$$d = t \alpha \left(1 - \frac{1}{n'} \right) \quad (7)$$

It is clear from this equation that the lateral displacement of the incident beam from the optical axis is proportional to the thickness of the refractor plate and to the angle it makes with the incident beam.

The lateral displacement of the image of the entrance slit at the exit slit plane in wavelength units, $\overset{\circ}{\text{A}}$, is

$$a = d R_d \quad (8)$$

where R_d is the reciprocal linear dispersion of the monochromator ($\overset{\circ}{\text{A}} \text{ mm}^{-1}$).

The result of oscillating the refractor plate periodically so that the angle of the incident beam varies periodically from α to $-\alpha$ at some angular frequency ω_2 is to oscillate the entrance slit image about some mean wavelength, λ_c , which corresponds to the position of the grating of the monochromator with the refractor plate perpendicular to the entering light beam. The position of the mobile spectrum with respect to the grating setting, λ_c , may be expressed as

$$\lambda = \lambda_c + a \sin \omega_2 t \quad (9)$$

where λ is the mean wavelength passing through the exit slit.

The Rayleigh scattering mentioned in the preceding section is accounted for by wavelength modulation. Since Rayleigh scattering is independent of wavelength over a small wavelength range for a given particle size, any scattering will be the same at the absorption line and close by it. Thus, there will be a constant difference between the baseline signal and the absorption signal whether scattering is present or not.

In addition to causing a lateral displacement of an axial beam incident upon it at some angle α , the refractor plate also causes a displacement of non-axial beams parallel to the optical axis, Figure 1b,

$$\delta = d / \sin \alpha \quad (10)$$

where δ is the parallel displacement of the image (mm). By substituting the small angle approximation for d and for $\sin \alpha$ the following result is obtained

$$\delta = t(1 - \frac{1}{n^2}) \quad (11)$$

For the case of quartz, this means that the image of the incident beam is displaced a distance of approximately one-third the thickness of the refractor plate. In practice the result is a slight defocussing of the exit image which can be neglected.

Intensity Expressions

Intensity expressions which allow quantitative prediction of experimental signals will be derived in the following section. It will be shown that signals corresponding to both first and second derivatives of the transmitted spectrum are predicted. The expressions derived for this system are general and apply equally to spectra containing narrow or broad lines.

The experimental arrangement for which the expressions will be derived is illustrated in Figure 2. The source employed must be a continuum for the expressions to hold. The source radiance and the radiance at each important point are also indicated in Figure 2.

Fig. 2.--Schematic diagram of the optical system.

$B_{\lambda_0}^0$ = Unmodulated source radiance (watts $\text{cm}^{-2}\text{sr}^{-1}\text{nm}^{-1}$).

$B_{\lambda_0}^c$ = Chopped source radiance (watts $\text{cm}^{-2}\text{sr}^{-1}\text{nm}^{-1}$).

$B_{\lambda_{\text{MT}}}^c$ = Transmitted radiance (watts $\text{cm}^{-2}\text{sr}^{-1}\text{nm}^{-1}$).

$B_{\text{T}}(\lambda_c, \nu)$ = Transmitted modulated spectrum (watts).

L_1 = Spectrosil lens, 3.2" focal length.

L_2 = Spectrosil lens, 2.4" focal length.

L_3 = Spectrosil lens, 2.7" focal length.

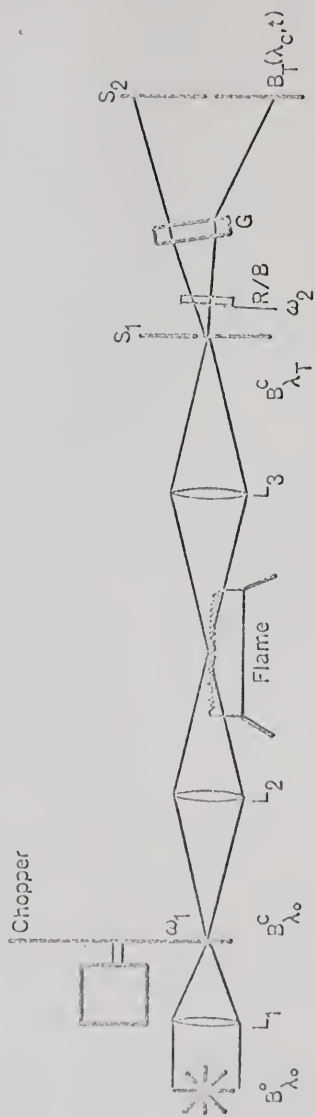
S_1S_2 = Entrance and exit slits of monochromator.

R/B = Refractor plate-piezoelectric bimorph combination.

G = Grating of monochromator.

ω_1 = Frequency of source modulation (sec^{-1}).

ω_2 = Frequency of wavelength modulation (sec^{-1}).



The continuum source spectral radiance, $B_{\lambda_0}^o$, is focussed onto the blade of a chopper wheel rotating at an angular frequency ω_1 . The modulated spectral radiance, $B_{\lambda_0}^c$, is then focussed onto a flame absorption cell into which analyte absorbing species may be introduced. The radiance transmitted through the absorption cell, $B_{\lambda_T}^c$, is related to the incident radiance, $B_{\lambda_0}^c$, by the absorption law [3,20]

$$B_{\lambda_T}^c = B_{\lambda_0}^c \exp(-\bar{k}_\lambda l) \quad (12)$$

where \bar{k}_λ is a modified atomic absorption coefficient defined by Equation (15) and l is the path length of the flame. Ordinarily, k_λ , the true atomic absorption coefficient for an atomic vapor is used in Equation (12) and is a function of wavelength; the peak atomic absorption coefficient, k_0 ; and the half-width of the absorption line, $\Delta\lambda_A$ [21]. However, when medium resolution monochromators having spectral bandwidths equal to or larger than the half-width of the absorption line are used, the apparent half-width of the spectral profile viewed by the monochromator is approximately the same as the spectral bandwidth [22]. The apparent half-width is herein defined as

$$\Delta = \sqrt{s^2 + \Delta\lambda_A^2} \quad (13)$$

Δ is the apparent half-width (\AA) and s is the spectral bandwidth of the monochromator (\AA)

$$s = R_d^1 W \quad (14)$$

In Equation (14), W is the slit width of the monochromator (cm) and R_d^1 is the reciprocal linear dispersion of the monochromator (\AA cm^{-1}). Furthermore, the value for k_0^{obs} , the peak atomic absorption coefficient at the line center, is also affected by the spectral bandwidth of the monochromator. Kostkowski and Bass [23] have calculated the change in k_0^{obs} for various spectral bandwidth-to-absorption line half-width ratios. For ratios greater than 2, which is generally the case for real analytical situations involving atomic lines, k_0^{obs} varies from 75 per cent to less than 50 per cent of the true k_0 . According to the above discussion, K_λ may be expressed as

$$K_\lambda = \rho k_0 \exp\left[-\frac{(\lambda - \lambda_0)^2}{\Delta}\right]^2 \quad (15)$$

where ρ is a coefficient less than 1.0 to account for the diminution of k_0^{obs} due to finite spectral bandwidth and λ_0 is the wavelength at the center of the absorption line profile. This expression only approximates reality since it describes a line having a Gaussian type of profile. However, considering the line as having a simple shape instead of its true shape which results from the several broadening processes occurring in flames, the expression becomes amenable to mathematical treatment. Equation (12) may be rewritten in a form which indicates more clearly that the exponential term simply expresses the transmission

of the flame cell as a function of wavelength

$$B_{\lambda T}^C = B_{\lambda_0}^O T(\lambda) \quad (16)$$

The radiance transmitted through the absorption cell is focussed upon the entrance slit of a monochromator after which it passes through a refractor plate modulated at an angular frequency ω_2 . The effect of the displacement of the image (described in the previous section) is to cause the spectrum produced by the grating of the monochromator to periodically oscillate about a mean wavelength, λ_c , corresponding to the central wavelength of the spectral band of radiation emerging from the exit slit when the monochromator is used in its conventional mode. The wavelength of the oscillating spectrum which is viewed by the center of the exit slit at any time t is given by Equation (9)

$$\lambda = \lambda_c + a \sin \omega_2 t$$

Therefore, the radiation emerging from the exit slit of the modulated system, $B_T(\lambda_c, t)$, is a function of the periodic oscillation of the spectrum about the center of the exit slit. Also, as a result of the finite width of the exit slit, $B_T(\lambda_c, t)$ is also a function of the spectral bandwidth of the monochromator. The modulated spectrum passing the exit slit may be expressed in the form of an integral of

$B_{\lambda T}^c$ convoluted with the slit function of the monochromator, $S(\lambda)$, evaluated over the spectral bandwidth of the monochromator

$$B_T(\lambda_c, t) = \int_{\lambda_c - s/2}^{\lambda_c + s/2} B_{\lambda T}^c S(\lambda) d\lambda \quad (17)$$

In the case of a monochromator having equal entrance and exit slits and unit magnification within the monochromator, $S(\lambda)$ is a triangular function and is expressed as

$$\begin{aligned} S(\lambda) &= 1 - \frac{|X|}{s}, \quad |X| = |\lambda - \lambda_c| < s \\ S(\lambda) &= 0, \quad |X| = |\lambda - \lambda_c| \geq s \end{aligned} \quad (18)$$

$B_{\lambda T}^c$ as expressed by Equation (16) may be rewritten as a function of the modulated spectrum and the slit width.

$$B_{\lambda T}^c = B_{\lambda_0}^c (\lambda_c + a \sin \omega_2 t + |X|) T(\lambda_c + a \sin \omega_2 t + |X|) \quad (19)$$

Substitution of Equations (18) and (19) into the integral of Equation (17) yields

$$B_T(\lambda_c, t) = \int_{\lambda_c - s/2}^{\lambda_c + s/2} B_{\lambda_0}^c (\lambda_c + a \sin \omega_2 t + |X|) T(\lambda_c + a \sin \omega_2 t + |X|) (1 - \frac{|X|}{s}) dX \quad (20)$$

A Taylor series expansion may be performed on the terms of Equation (19).

$$B_{\lambda_0}^c(\lambda) = B_{\lambda_0}^c(\lambda_c) + (a \sin \omega_2 t + |X|) B_{\lambda_0}^{c'}(\lambda_c) +$$

$$\frac{(a \sin \omega_2 t + |X|)^2}{2} B_{\lambda_0}^{c''}(\lambda_c) + \dots$$

$$T(\lambda) = T(\lambda_c) + (a \sin \omega_2 t + |X|) T'(\lambda_c) +$$

$$\frac{(a \sin \omega_2 t + |X|)^2}{2} T''(\lambda_c) + \dots \quad (21)$$

where the primes indicate the derivative of the expression with respect to λ evaluated at λ_c . For the purposes of arriving at the desired expression in this derivation, the expansion was only carried to the second order in $(a \sin \omega_2 t + |X|)$. A more precise expression could be obtained by expanding the series to higher order terms, but it will be shown that, for practical purposes, second order terms are sufficient and can either be accounted for experimentally or are negligible. Multiplication of all terms and subsequent integration over the spectral bandwidth results in the expression (see Table 1)

TABLE 1
BREAKDOWN OF INTENSITY EXPRESSION $B_T(\lambda_c, \nu)$

Frequency Dependence of Terms	Terms	Comments
dc Terms	$sB + \frac{sa^2}{4} (B'' + 2B'' + B''')$	Not detected by AC system
First Harmonic Terms	$(\frac{saB''}{2} + saB'' + \frac{2sa^3}{8} B''') + \frac{2sa^3}{8} B''') \sin \omega_2 \nu$	First term yields first derivative of transmitted spectrum at detection frequency of ω_2
Second Harmonic Terms	$(\frac{sa^2B''}{4} + \frac{sa^2B''}{2} + \frac{sa^2B''}{4}) \sin 2\omega_2 \nu$	First term yields second derivative of transmitted spectrum at detection frequency of $2\omega_2$

Note: All terms other than those underlined are constant or negligible. See text for explanation.

$$\begin{aligned}
B_T(\lambda_c, t) = & sBT + \frac{sa^2}{4} (BT'' + 2B'T' + B''T) \\
& + sa \sin \omega_2 t [BT' + B'T + \frac{a^2}{8} (3B'T'' + 5B''T')] \\
& + \frac{sa^2}{4} \sin 2\omega_2 t [BT'' + 2B'T' + B''T] \\
& + \text{higher harmonics} \qquad (22)
\end{aligned}$$

where all superscripts and subscripts have been omitted to simplify the expression.

The first two terms of the expression represent the dc signal output of the multiplier phototube detector.

Of the terms appearing at the fundamental frequency ω_2 , the first term describes the first derivative of the transmitted spectrum; the second term is zero if the source radiance is constant or a constant if the radiance increases or decreases linearly over the spectral modulation interval, a ; the third term is zero at the wavelength of the first derivative maximum and the fourth term is zero if the source spectrum has no fine structure over the spectral modulation interval.

Of the terms appearing at the second harmonic, $2\omega_2$, the first describes the second derivative of the transmitted spectrum; the second is zero at the wavelength of the second derivative maximum; the third is zero if the source spectrum has no fine structure over the spectral modulation interval.

Subject to the above conditions, only two terms in the entire expression are important in the ac detection mode. These are the first term at the fundamental frequency

$$sa \sin \omega_2 t B_{\lambda_0}^c(\lambda_c) T'(\lambda_c) \quad (23a)$$

and the first term at the second harmonic frequency

$$\frac{sa^2}{4} \sin 2\omega_2 t B_{\lambda_0}^c(\lambda_c) T''(\lambda_c) \quad (23b)$$

Each of these expressions may be expanded by substitution of the appropriate derivatives.

$$\begin{aligned} T(\lambda) &= \exp(-\bar{k}_\lambda l) \\ T'(\lambda) &= -\frac{d\bar{k}_\lambda}{d\lambda} l \exp(-\bar{k}_\lambda l) \\ T''(\lambda) &= -\frac{d^2\bar{k}_\lambda}{d\lambda^2} l \exp(-\bar{k}_\lambda l) + \left(\frac{d\bar{k}_\lambda}{d\lambda} l\right)^2 \exp(-\bar{k}_\lambda l) \end{aligned} \quad (24)$$

Substitution into the expressions (24) may be accomplished by taking the appropriate derivatives of Equation (15).

$$\frac{d\bar{k}_\lambda}{d\lambda} = -\frac{2\rho k_0}{\Delta^2} (\lambda - \lambda_0) \exp - \left[\frac{\lambda - \lambda_0}{\Delta} \right]^2 \quad (25a)$$

$$\begin{aligned} \frac{d^2\bar{k}_\lambda}{d\lambda^2} &= -\frac{2\rho k_0}{\Delta^2} \exp - \left[\frac{\lambda - \lambda_0}{\Delta} \right]^2 + \frac{4\rho k_0}{\Delta^4} (\lambda - \lambda_0)^2 \cdot \\ &\quad \exp - \left[\frac{\lambda - \lambda_0}{\Delta} \right]^2 \end{aligned} \quad (25b)$$

By substituting expressions 25a and 25b into expressions 24 and evaluating at λ_c one obtains

$$T'(\lambda_c) = \frac{2\rho k_0}{\Delta^2} 1(\lambda_c - \lambda_0) \exp - \left[\frac{\lambda_c - \lambda_0}{\Delta} \right]^2 \exp(-\bar{k}_\lambda 1) \quad (26)$$

and

$$T''(\lambda_c) = \left\{ \frac{2\rho k_0}{\Delta^2} 1 \exp - \left[\frac{\lambda_c - \lambda_0}{\Delta} \right]^2 + \frac{4\rho k_0}{\Delta^4} 1(\lambda_c - \lambda_0)^2 \exp - \left[\frac{\lambda_0 - \lambda_c}{\Delta} \right]^2 + \left[\frac{2\rho k_0}{\Delta^2} 1(\lambda_c - \lambda_0) \exp - \left[\frac{\lambda_c - \lambda_0}{\Delta} \right]^2 \right]^2 \right\} \exp(-\bar{k}_\lambda 1) \quad (27)$$

The location of the maxima or minimum of Equation (25a) can be found by setting Equation (25b) to zero, substituting λ_c for λ and solving for λ_c . At the maximum or minimum

$$\lambda_c = \lambda_0 \pm \frac{\Delta}{\sqrt{2}} \quad (28)$$

The maxima or minima of Equation (27) can be located by setting $\frac{d^3 \bar{k}_\lambda}{d\lambda^3}$ equal to zero and solving for λ_0 . Three values are obtained, of which $\lambda_c = \lambda_0$ is the maximum.

$$\begin{aligned} \lambda_c &= \lambda_0 \\ \lambda_c &= \lambda_0 \pm \sqrt{5/2} \Delta \end{aligned} \quad (29)$$

When Equation (26) is evaluated at $\lambda_c = \lambda_0 + \frac{\Delta}{\sqrt{2}}$, it becomes

$$T'(\lambda_c) = \frac{2\rho k_0}{\sqrt{2}\Delta} 1 \exp(-j/2) \exp(-\bar{k}_\lambda l) \quad (30)$$

Evaluating Equation (27) at $\lambda_c = \lambda_0$ one obtains

$$T''(\lambda_c) = \frac{2\rho k_0}{\Delta} 1 \exp(-\bar{k}_\lambda l) \quad (31)$$

These expressions may be substituted back into Equations (23a) and (23b) and Equation (1) substituted for $B_{\lambda_0}^c$. When this is done, Equation (23a) becomes

$$\begin{aligned} sa \cdot \sin \omega_2 t \left[B_{\lambda_0}^c(\lambda_c) T'(\lambda_c) \right] &= sa \cdot \sin \omega_2 t \left[\frac{1}{2} B_{\lambda_0}^o (1 + \right. \\ &\quad \left. \cos \omega_1 t) \frac{2\rho k_0}{\sqrt{2}\Delta} 1 \exp(-j/2) \exp(-\bar{k}_\lambda l) \right] \end{aligned}$$

Multiplying through and discarding any terms not having both ω_1 and ω_2 appearing in them, one obtains

$$\begin{aligned} sa \cdot \sin \omega_2 t \left[B_{\lambda_0}^c(\lambda_c) T'(\lambda_c) \right] &= \left[\sin(\omega_1 + \omega_2) t + \right. \\ &\quad \left. \sin(\omega_1 - \omega_2) t \right] \frac{sa B_{\lambda_0}^o \rho k_0 1 \exp(-j/2) \exp(-\bar{k}_\lambda l)}{2\sqrt{2}\Delta} \end{aligned} \quad (32)$$

Equation (32) predicts that the first derivative of the transmitted spectrum should appear at both the sum and the difference of the modulation frequencies. Similar substitution can be made into Equation (23b) with the result

being

$$sa^2 \sin 2\omega_2 t \left[B_{\lambda_0}^0(\lambda_c) u''(\lambda_c) \right] = \left[\sin(\omega_1 + 2\omega_2)t + \sin(\omega_1 - 2\omega_2)t \right] \frac{sa^2 B_{\lambda_0}^0 \rho k_0 l \exp(-\bar{k}_\lambda l)}{8 \Delta^2} \quad (33)$$

Equation (33) predicts that the second derivative of the transmitted spectrum should appear at the sum of the chopping frequency and twice the wavelength modulation frequency and also at their difference. Examples of first and second derivative signals are shown in Figure 3.

Equations (32) and (33) may now be written as input signals to the phase lock amplifier at their appropriate frequencies of detection and phase so that the sin terms are equal to unity.

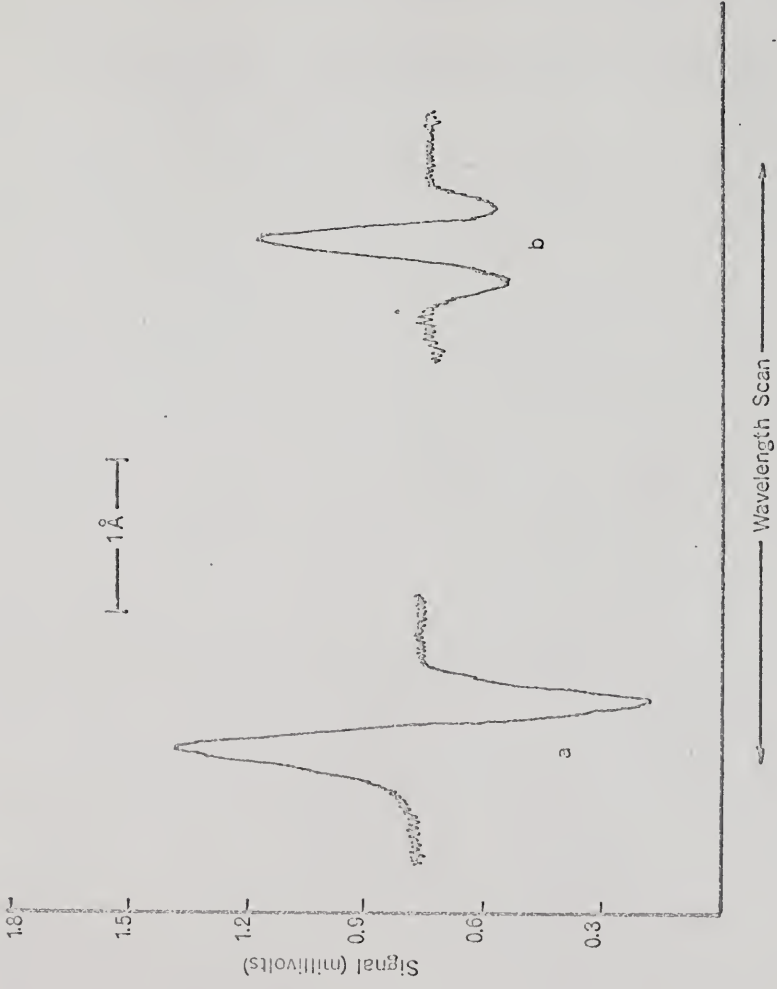
$$S_{\omega_1 + \omega_2} = \frac{WH \Omega_{II} T_F \gamma R_L sa B_{\lambda_0}^0 \rho k_0 l \exp(-1/2) \exp(-\bar{k}_\lambda l)}{2 \sqrt{2} \Delta} \quad (34)$$

where W and H are the width and height of the monochromator slit, respectively, in cm, Ω_{II} is the solid angle of radiation collected by the monochromator in steradians, T_F is the transmission factor of the optics of the system, γ is the phototube radiant sensitivity in amperes watt⁻¹, and R_L is the phototube load resistor in ohms.

$$S_{\omega_1 + 2\omega_2} = \frac{WH \Omega_{II} T_F \gamma R_L sa^2 B_{\lambda_0}^0 \rho k_0 l \exp(-\bar{k}_\lambda l)}{8 \Delta^2} \quad (35)$$

FIG. 3a.---First derivative of Ca resonance line profile at 4227 \AA
at a concentration of $25 \mu\text{g ml}^{-1}$.

FIG. 3b.---Second derivative of Ca resonance line profile at 4227 \AA
at a concentration of $25 \mu\text{g ml}^{-1}$.



Equations (34) and (35) predict that the first derivative signal should be larger than the second by the ratio

$$\frac{S_{\omega_1 + \omega_2}}{S_{\frac{\omega_1 + \omega_2}{2}}} = \frac{24\sqrt{2}}{a} \exp(-\frac{1}{2}) \quad (36)$$

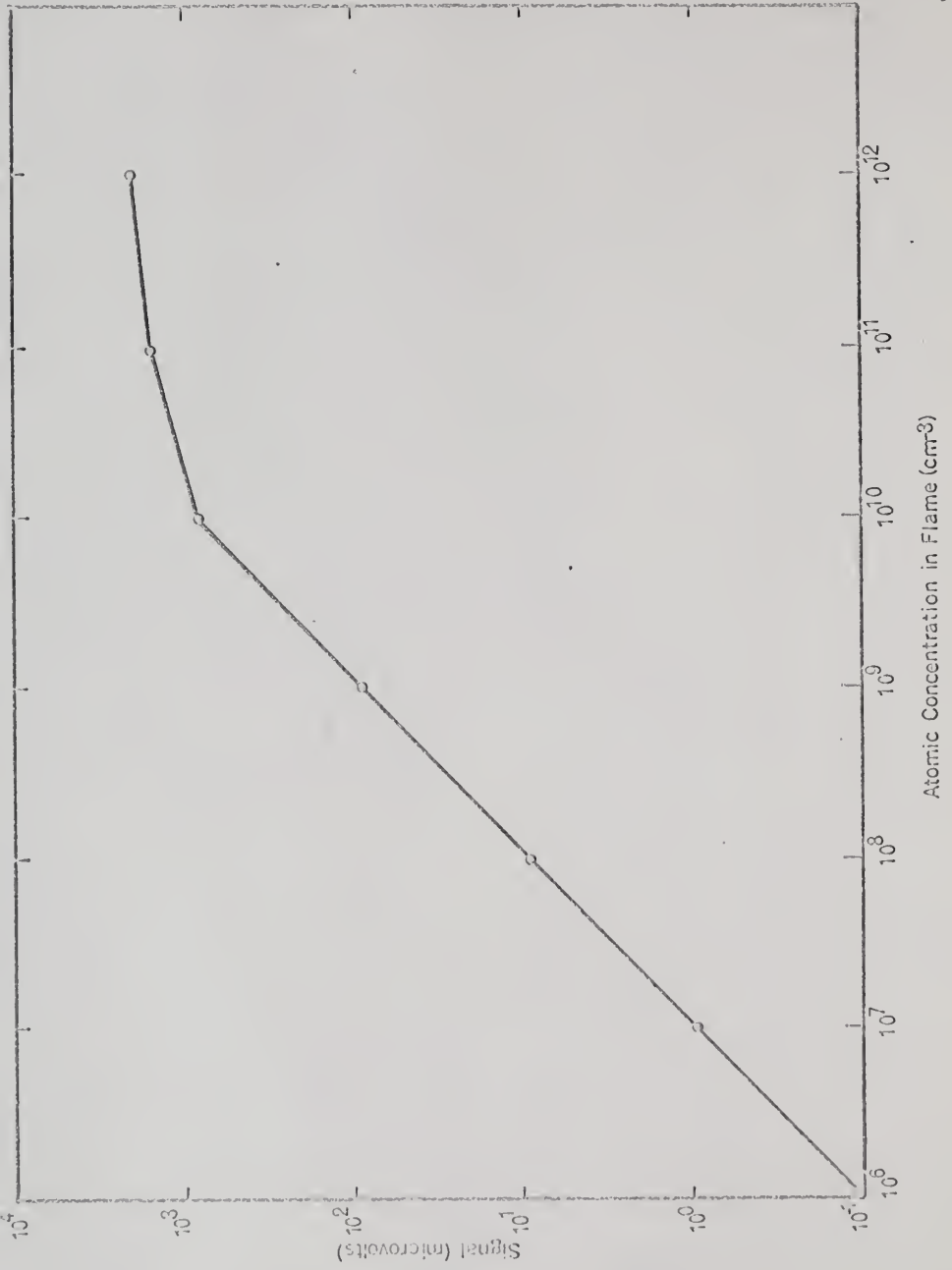
They represent the final expressions which are used to predict the shape of the curves of growth for the derivative system. A theoretical first derivative growth curve is shown in Figure 4.

That there is an optimum spectral modulation amplitude is shown by Balslev [13] who gives the resolution for a conventional monochromator as $\frac{s_1 + s_2}{2} = s$ where s_1 and s_2 are the spectral slit widths of the entrance slit and exit slit, respectively. For the case of a monochromator modified to produce a derivative signal and having a spectral modulation amplitude s_3 the resolution is given as

$$\frac{s_1 + s_2 + s_3}{2} = s \quad (37)$$

Since the signal of the derivative spectrometer, according to Balslev, is proportional to $s_1 s_2 s_3$, the best choice for slit widths and modulation amplitude for optimum resolution and signal is $s_1 = s_2 = s_3$. In the preceding derivation,

Fig. 4.--Theoretical curve of growth for Ca at 4227 \AA by first derivative analysis.



the assumption that $s_1 = s_2$ has already been made. Considering now the size of s_3 one sees that if $s_3 < s_1$ resolution will be improved but the signal will decrease and if $s_3 > s_1$ the signal will increase but resolution will suffer. In the previous equations, a is equivalent to s_3 . For the optimum case a should be chosen equal to s_1 . Equation (36) then predicts that the ratio of the first to second derivative signals should be 1.7.

Limits of Detection

Winefordner and Vickers [20] have derived expressions for calculating the theoretical concentration of analyte at the limit of detectability in atomic absorption flame spectrometry for a system employing a hollow cathode discharge lamp as a source and dc detection of the signal. In their derivation, they defined the limit of detectability as the concentration of analyte atoms in a flame which produces a change in signal equal to twice the root-mean-square noise signal due to all sources of noise present in the system. The major sources of noise present in any system are (i) fluctuations in the signal arising from the photodetector or photon noise; (ii) fluctuations in signal arising from source intensity fluctuations or source flicker noise, and (iii) fluctuations in the signal arising from fluctuations in the intensity of background flame emission intensity or flame flicker noise. Of these sources of noise, flame

flicker and source flicker noises are of the "pink" or $1/f$ variety, that is, they are less than 100 Hz. Photon noise, on the other hand, is "white" noise, that is, the spectral noise power is approximately constant over the entire frequency spectrum. Therefore, one should expect to encounter only photon noise in ac detection systems operating at frequencies greater than about 100 Hz. The following derivation of the analyte concentration at the limit of detectability is based on the assumption that the system is photon noise limited. The photoanodic current due to photon noise may be written as [20]

$$\bar{\Delta i}_p = \sqrt{2BMe\Delta f VWH\Omega_{\text{eff}} T B \lambda_0^c} \quad (38)$$

where B is a factor characteristic of the photodetector dynodes, M is the multiplication (amplification) factor of the photodetector, e is the charge on the electron (coulombs), Δf is the frequency response bandwidth (sec^{-1}), and all other terms have been previously defined. Because photon noise is frequency independent, it will be detected along with the signal. At the limit of detectability, the signal due to analyte absorbing species will be equal to twice the photon noise. For the first derivative system

$$S_{\omega_1 + \omega_2}^{\text{min}} = 2R_L \bar{\Delta i}_p \quad (39)$$

The term in the signal expression (Equation 34) which relates the signal size to the number of analyte absorbers is k_o . The value of k_o^{\min} for the minimum detectable number of atoms in the flame, n_m^i , is given by [21]

$$k_o^{\min} = \frac{2 \sqrt{\ln 2} (\lambda_o)^2 \pi e^2 n_m^i f}{\sqrt{\pi} \Delta \lambda_D mc^2} \quad (40)$$

where n_m^i is the minimum detectable number of atoms in the i th state per cm^3 of flame gases, $\Delta \lambda_D$ is the Doppler half-width (\AA), f is the oscillator strength for the atomic transition and c is the speed of light (cm sec^{-1}). n^i may be calculated using the Boltzmann Equation (20)

$$n^i = \frac{ng_i}{Z(T)} \quad (41)$$

where n is the total number of atoms in all states; g_i is the statistical weight of state i , $2J + 1$; and $Z(T)$ is the partition function of the atom, $Z(T) = \sum_i g_i \exp(-E_i/kT)$, where E_i is the energy of state i above the ground state, k is the Boltzmann constant, T is the absolute temperature, and the summation is over all states of the atom.

Equations (34,38,40 and 41) may be substituted into Equation (39) and the resulting expression solved for n_m to yield a general equation for the minimum number of atoms detectable in a flame.

$$n_m = \frac{Z(T)}{\epsilon_i} \cdot \frac{2\Delta\lambda_D c}{\frac{\pi e^2}{mc} \rho(\lambda_0)^2 f l \exp(-1/2)} \cdot \left[\frac{2\pi B h c \Delta f}{\ln 2 W H \Omega_M T_1 B \lambda_0^0 \text{ s} \gamma} \right]^{1/2} \quad (42)$$

The minimum detectable concentration of atoms cm^{-3} of flame gases, n_m , can be converted to minimum detectable solution concentration in $\mu\text{g ml}^{-1}$, C_m , by use of the following Equation [20].

$$C_m = \frac{3.3 \times 10^{-19} n_m T Q n_T}{\phi \epsilon \beta n_{298}} \cdot A \quad (43)$$

where T is the flame temperature in $^{\circ}\text{K}$; n_T is the number of moles of combustion products at temperature T ; n_{298} is the number of moles present at 298°K ; Q is the flow rate of unburned gases in $\text{cm}^3 \text{sec}^{-1}$ at room temperature and one atmosphere pressure; ϕ is the flow rate of solution in $\text{cm}^3 \text{minute}^{-1}$; ϵ is the efficiency of atomization and nebulization processes; β is a factor to account for incomplete dissociation and atomic losses due to ionization; and the atomic weight is expressed in grams mole $^{-1}$, and A is the atomic weight of the analyte. The constant contains the numerical factors 298°K , Avogadro's number and conversion factors from minutes to seconds and from grams to micrograms. It thus has units of (moles atom $^{-1}$) (seconds minute $^{-1}$) (micrograms gram $^{-1}$) ($^{\circ}\text{K}^{-1}$).

Signal-to-Noise Ratio

The signal-to-noise ratio of the system in the first derivative mode is written as

$$S/N = \left[\frac{W H_0 T_f B_\lambda^0 \gamma E M \Delta f s}{4} \right]^{1/2} \rho k_o l \cdot \exp(-1/2) \exp(-\frac{k_\lambda l}{\lambda}) \quad (44)$$

Equation (44) predicts that the signal-to-noise ratio will improve with the square root of the source intensity.

CHAPTER III

EXPERIMENTAL SYSTEM AND PROCEDURES

Description of System

The instrumental system is pictured in a block diagram in Figure 5. Each of the individual components is discussed in detail below. The entire system was mounted on a one inch thick steel plate using quick-release magnetic mounts. This arrangement facilitated the location and physical stabilization of components while at the same time allowing rapid and easy experimental rearrangement. Components used are listed in Tables 2 and 3.

Source

Continuum sources were employed in all of the experiments. A 150 watt high pressure xenon arc having a collimated beam was used for all analytical experiments. The spectral distribution of radiant flux for the lamp as given by the manufacturer's specifications is shown in Figure 6. Source intensity below 3200 \AA is only about one-tenth of the output around 4500 \AA . Since most atomic resonance lines for elements which ordinarily are measured by atomic absorption

Fig. 5.--Block diagram of experimental system.

S = Source.

PMT = 1P28A multiplier phototube.

R/B = Refractor plate-piezoelectric bimorph combination.

L_1, L_2, L_3 = Spectrosil lenses.

R_L = Phototube load resistor.

ω_1 = Frequency of source modulation.

ω_2 = Frequency of wavelength modulation.

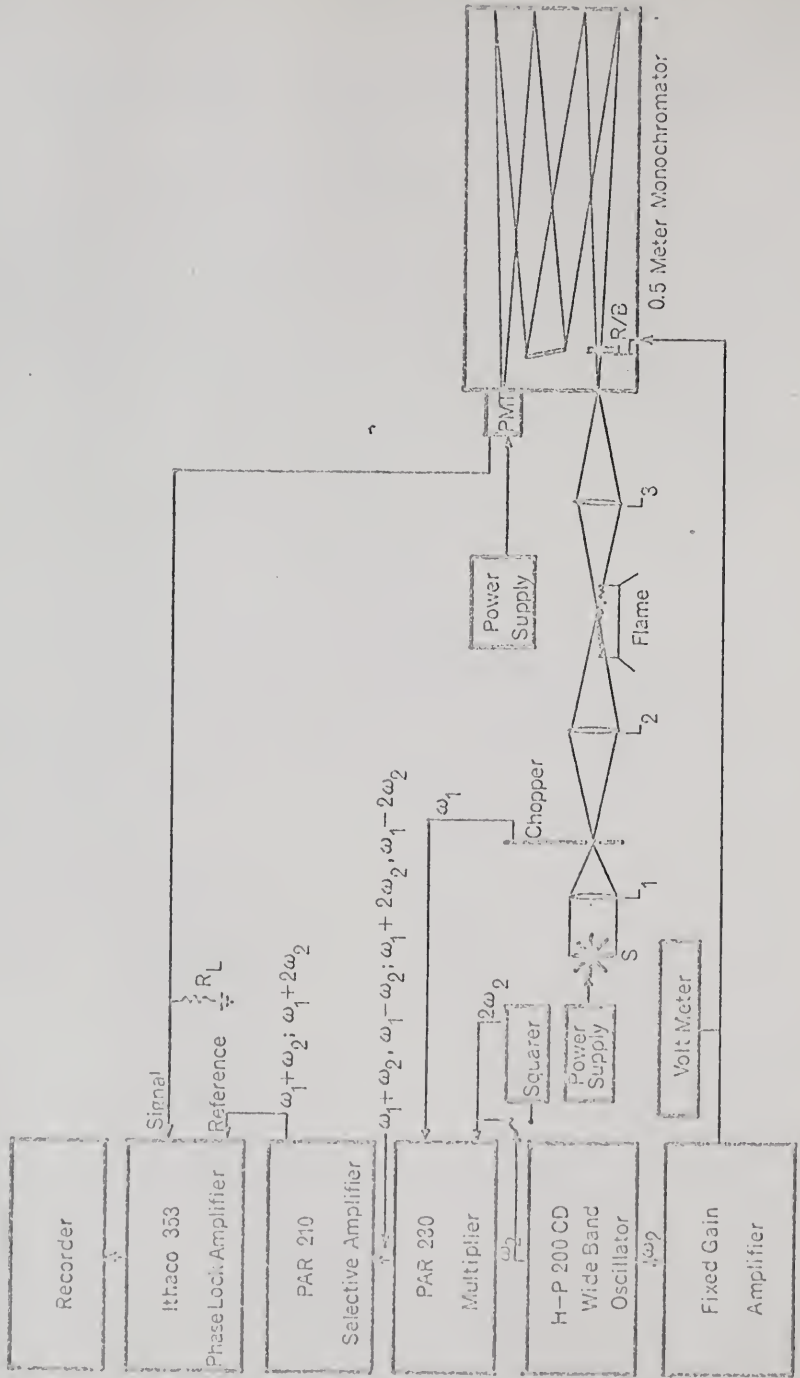


TABLE 2

OPTICAL COMPONENTS

Component	Type and/or Description	Supplier
Source	Model 150X88, 150 watt xenon arc with parabolic silver reflector, collimated beam Type FCS, 150 watt tungsten-halogen lamp operated at 24 volts	Varian, Elmac Div. 301 Industrial Way San Carlos, Calif. General Electric Co. Photo Lamp Dept. Mela Park Cleveland, Ohio
Xenon Arc Source Power Supply	Model P 250S-2, Illuminator Power Supply	Varian, Elmac Div. 301 Industrial Way San Carlos, Calif.
Tungsten Halogen Lamp Power Supply	Type CVN-1, Constant voltage transformer Class A, Type 1 24 volt, 10 amp step-down transformer	Sola Electric Co. Elk Grove Village, Ill. Freed Transformer Co., Inc., Brooklyn, N.Y.
Nebulizer	Type 303-0110 adjustable nebulizer and mixing chamber	Perkin-Elmer Corp. Norwalk, Conn.
Burner	Type 303-0401 three-slot Boling burner	Perkin-Elmer Corp. Norwalk, Conn.

Table 2 (Cont'd)

Component	Type and/or Description	Supplier
Monochromator	Type 82-000, 0.5 meter Ebert mount scanning monochromator with bilateral adjustable curved slits	Jarrell-Ash Corp. 590 Lincoln St. Waltham, Mass.
Gratings	Type 13701, 1180 grooves/mm., 52 mm x 52 mm, blazed at 5000 Å	Jarrell-Ash Corp. 590 Lincoln St. Waltham, Mass.
Laser	Model 310, Helium-Neon laser, 0.3 milliwatts	Metrologic Instrument 145 Harding Ave. Bellmawr, N.J.
Lenses	2 inch diameter, bi-convex Spectrosil lenses with the following focal lengths L1 = 3.2 inches L2 = 2.4 inches L3 = 2.7 inches	Esco Products Oak Ridge, N.J.
Refractor Plate	Suprasil quartz plate, 1.5 inches x 0.5 inches x 0.125 inches	Esco Products Oak Ridge, N.J.
Piezoelectric Bimorph	Type PZT - 5, 1.25 inches x 0.5 inches x 0.021 inches	Gould, Inc. Piezoelectric Div. 232 Forbes Road Bedford, Ohio

TABLE 3

ELECTRICAL COMPONENTS

Component	Type and/or Description	Supplier
Wide Band Oscillator	Model 200 CD Wide Band Oscillator	Hewlett-Packard Co. 1501 Page Mill Rd. Palo Alto, Calif.
Multiplier Unit	Model 230, Multiplier Unit, A x B mode	Princeton Applied Research Corp. Princeton, N.J.
Squarer	Model 426 Wide Band Four Quadrant Multiplier-Divider Square Rooter powered by Model 904 Dual Op Amp Power Supply	Analog Devices Cambridge, Mass.
Selective Amplifier	Model 210, Selective Amplifier	Princeton Applied Research Corp. Princeton, N.J.
Phase-Lock Amplifier	Model 353 Phase Lock Amplifier with Type B1 Amplifier, C1 Demodulator, and Display Module	Ithaca, Inc. 413 Taughannock Blvd. Ithaca, N.Y.
Multiplier Phototube	RCA 1P28A having S-5 response operated at -800 volts	Heath Co. Benton Harbor, Mich.

Table 3 (cont'd)

Component	Type and/or Description	Supplier
Phototube Power Supply	Model 26-770 High Voltage Power Supply	Jarrell-Ash Corp. 590 Lincoln St. Waltham, Mass.
Recorder	Model SR 10 inch chart recorder with 10 mv. adapter, 3-speed drive	Sargent-Welch Scientific Co. 3125 7th Ave. Birmingham, Ala.

Fig. 6.--Relative spectral radiance of xenon arc.

----- Manufacturer's specifications.

- - - Experimental results.



techniques fall below 3600 \AA (Al, Ba, Ca, Cs, K, Li, Na, Rb, Sr and most rare earths have useful resonance lines above 3600 \AA), a very powerful source is required to yield appreciable intensity in this low wavelength region of the spectrum. The xenon arc source used had an effective spectral radiance in the region of 4000 \AA of between 10^{-4} and $10^{-3} \text{ watts cm}^{-2} \text{ sr}^{-1} \text{ nm}^{-1}$ and correspondingly lower spectral radiance at the lower wavelength resonance lines. The measured spectral radiance of the source at the wavelengths employed is also plotted in Figure 6 as relative values. The spectral radiance at 4227 \AA is arbitrarily assigned a value of 1. The estimation of source spectral radiance was made by measuring the phototube signal which resulted when the source was focussed on the slit of the monochromator under known conditions. Equation (45) was used to calculate $B_{\lambda_0}^{\circ} T_F$. The transmission factor was included in the calculated value since an accurate estimation of its value could not be made; however, all other parameters were known.

$$\text{Signal} = B_{\lambda_0}^{\circ} T_F W H \Omega_M s \quad (45)$$

where the signal is the phototube signal in amperes; W and H are the width and height of the monochromator slits, respectively, in cm; Ω_M is the solid angle of radiation collected by the monochromator in steradians; s is the

spectral bandwidth of the monochromator in nm; and \mathcal{V} is the radiant sensitivity of the phototube in amperes watt⁻¹.

Source flicker was not observed to be a problem. This finding is in agreement with Snelleman [17] and others [24] who have shown that source flicker at frequencies greater than 100 Hz is negligible.

A tungsten-iodine projector lamp having a quartz envelope was used in an experiment to verify photon noise limitations. Its power supply is indicated in Table 2.

Burner and Nebulizer

An adjustable nebulizer and mixing chamber assembly was employed in all experiments. The efficiency of the nebulizer in delivering aspirated sample into the flame was on the order of 5 to 10 per cent. The nebulizer chamber was equipped with a 3-slot burner head 10 cm in length. The burner supported an acetylene-air flame for all experimental measurements. The entire nebulizer-burner assembly was mounted on an aluminum shaft which could be set at various heights by means of an adjustable locking collar. The collar was mounted on a quick-release magnetic mount which allowed rapid alignment of the burner head with respect to the optical axis of the system.

Monochromator and Optics

A 0.5 meter scanning Ebert monochromator was employed in this study. It was mounted on a 1 inch thick aluminum plate which was supported by three adjustable posts mounted on quick-release magnetic mounts. The monochromator was initially roughly leveled using a spirit level while precise leveling was accomplished by using a small, low-power helium-neon laser. The laser was set to the appropriate height and its beam made parallel to the steel plate by the use of glass plates which were epoxied to adjustable rods mounted on quick-release magnetic mounts and which had an "X" inscribed on one face. These were positioned such that the centers of the "X"'s coincided with the horizontal plane containing the optical axis of the system. By placing these in the path of the laser beam at various distances from the laser aperture, the laser could easily be adjusted so that the beam coincided with the centers of the "X"'s and thus was contained in the optical plane of the system. The monochromator was leveled by illuminating the center of the entrance slit with the leveled laser beam and adjusting the height and level of the monochromator until the beam emerging from the exit slit was contained in the optical plane.

The lenses used to focus the source radiation were aligned in the same manner as the monochromator. They were

placed in approximately their final position on the optical bench and adjusted vertically until their centers were contained in the optical plane as indicated by their transmission of the laser beam. Initially, their position along the optical axis was defined by the criterion of obtaining a 1:1 image of the source at the entrance slit. When this arrangement was made, it was discovered that the center of the grating was dark as were the centers of the collimating mirrors of the monochromator. Due to the construction of the source, this phenomenon was understandable. The anode of the lamp is supported by a metal spider mounted immediately behind the sapphire front window and is directly in front of the arc. This unilluminated portion of the source image coincides with its center and accounts for the dark areas observed. To correct this problem, a demagnified image of the source was formed on the slit by relocation of the lenses with subsequent complete illumination of the grating.

The quartz refractor plate used to displace the image of the entrance slit was mounted in a brass electrode holder as shown in Figure 7. The electrode holder was located on the monochromator chassis at a distance from the entrance slit such that the width of the plate was sufficient to totally intersect the solid angle of radiation collected by the collimator mirror. The refractor plate was epoxied to a

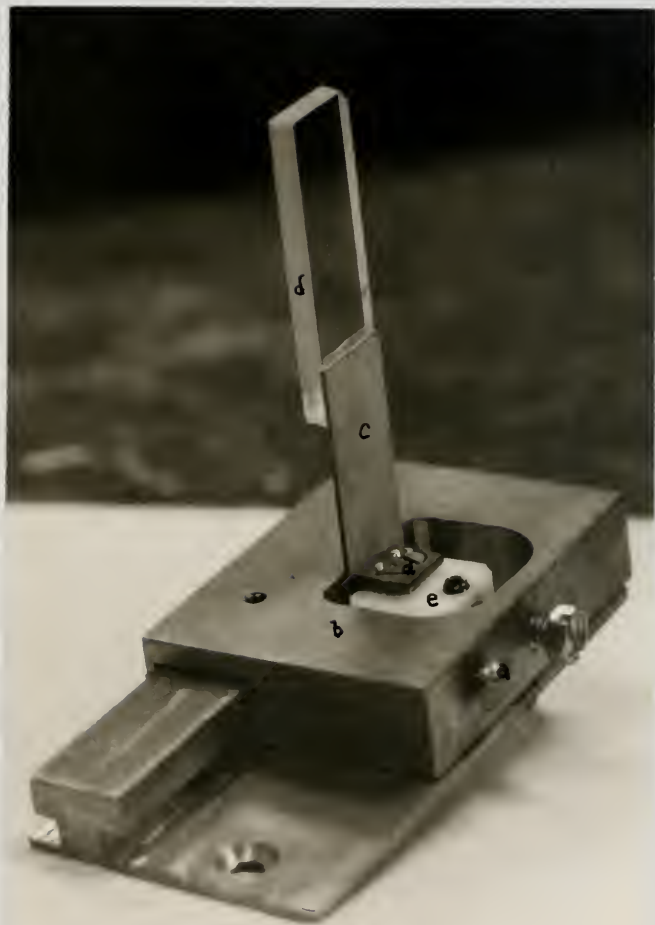


Fig. 7.--Electrode holder for piezoelectric transducer.

- a = Brass electrodes.
- b = Brass holder block.
- c = Piezoelectric bimorph transducer.
- d = Quartz refractor plate.
- e = Teflon[®] insulator block.

piezoelectric bimorph. Oscillation of the refractor plate was accomplished by supplying the piezoelectric bimorph with a sinusoidally varying voltage. The optimum performance of the piezoelectric bimorph was expected to occur at its resonance frequency. The approximate resonance frequency was calculated using Equation (46) [25,26]

$$\omega = \frac{350}{L^2} \quad (46)$$

where L is the free length of the vibrating member in inches; ω was calculated to be 56 Hz. Experimentally the resonance frequency was found to be 55 Hz. Consequently, the bimorph was driven at 55 Hz by a voltage of the appropriate magnitude to attain the desired deflection and thereby the desired spectral modulation interval (Figure 8).

The mechanical chopper used to interrupt the source radiation falling on the flame was constructed in the chemistry department machine shop. It consisted of an 8 inch diameter wheel having 10 apertures driven by a synchronous 3600 rpm motor. The ratio of the motor pulley wheel to the chopper blade pulley wheel was 0,430 which resulted in a chopping frequency of 258 Hz.

A reference signal of this frequency was generated by a small photodetector system built into the chopper housing. The reference system used a 6.2 volt radio lamp and a phototransistor in the circuit diagrammed in Figure 9.

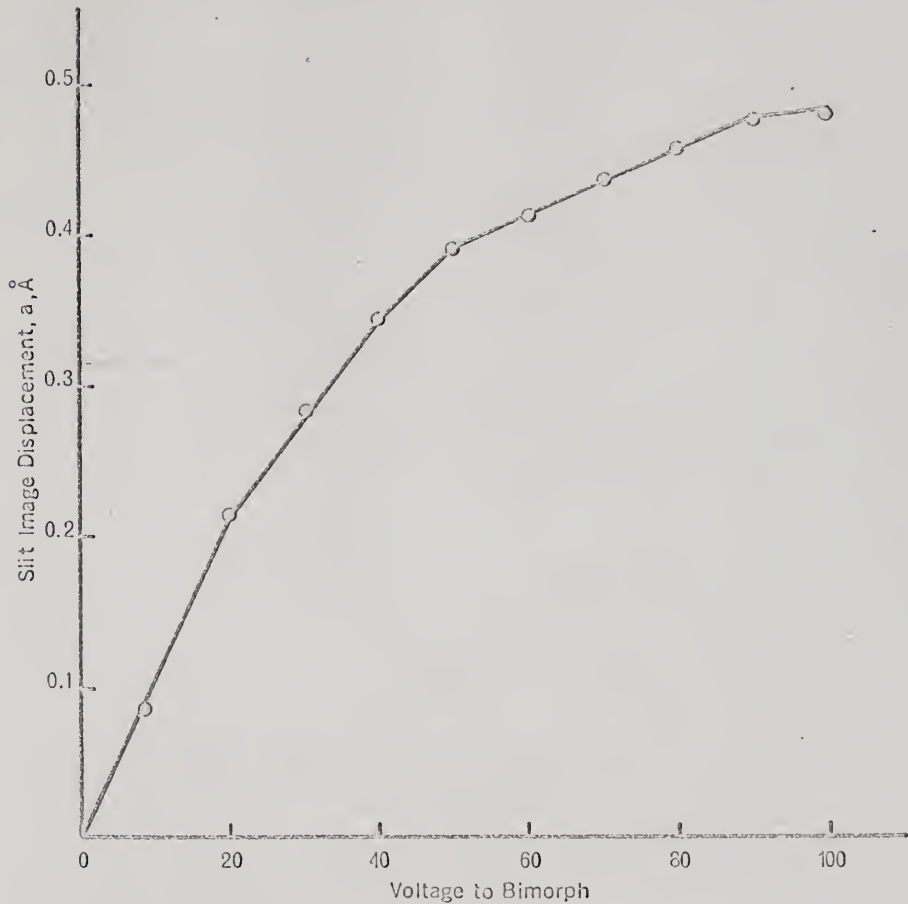


Fig. 8.--Spectral modulation amplitude (slit image displacement) versus voltage supplied to the bimorph.

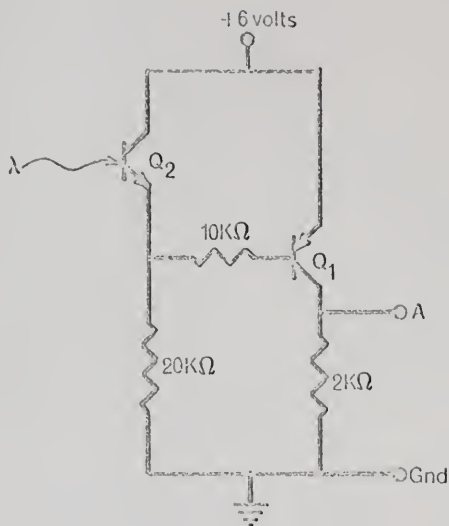


Fig. 9.---Circuit for chopper reference signal.

Q_1 = 2N5142.

Q_2 = LS400 (Texas Instrument, Inc.) phototransistor.

λ = Radiation incident on phototransistor.

A = Signal output.

The lamp and phototransistor were mounted beside each other on the face plate of the chopper housing. Directly opposite them a mirror was attached to the rear plate of the housing. When an aperture presented itself between the lamp and the mirror, light was reflected onto the phototransistor, its resistance decreased to a low value causing Q_1 to turn off. When Q_1 was off, point A dropped to zero volts. As an opaque portion of the chopper interrupted the light falling on the phototransistor, its resistance became high, Q_1 was turned on and point A rose to 6 volts. In this manner, an approximate square wave signal of frequency ω_1 was generated at point A for each interruption of the xenon source.

Electronic Components

The driving voltage to the piezoelectric bimorph was supplied at the proper frequency by using a variable amplitude wide band oscillator feeding into a fixed gain power amplifier which was capable of supplying up to 120 volts (rms) without distortion of the output wave form. The amplifier used in this experiment was constructed in the chemistry department electronics shop and not optimized to the load which the piezoelectric presented.¹

¹A suitable commercial amplifier would be the Model DCA-10, Krohn-Hite Power Amplifier, Krohn-Hite Corp., 580 Massachusetts Ave., Cambridge, Massachusetts.

The reference signal for the piezoelectric transducer frequency, ω_2 , was taken at the oscillator output. When the system was operated in the first derivative mode, this signal and the reference signal from the mechanical chopper were used as inputs to a multiplier. The result of multiplying two periodic functions together is given by Equation (47)

$$\sin(a) \cos(b) = \frac{1}{2}(\sin(a+b) + \sin(a-b)) \quad (47)$$

In the present system, the frequency of the multiplier output was of interest because it was to be used to supply the reference signal to the phase-lock amplifier. In order to differentiate between the sum and difference frequencies in the multiplier output, a tuned amplifier of high Q was used to select the proper frequency to be used as the reference signal to the lock-in. For the first derivative spectrum, the sum frequency was 313 Hz and the difference frequency was 203 Hz.

For operation of the system in the second derivative mode, the reference signal from the oscillator was fed into a squarer to obtain a signal at twice the oscillator frequency, $2\omega_2$. The output of the squarer and the chopper reference signal were fed into the multiplier as for first derivative operation and the selective amplifier tuned appropriately to either 368 Hz($\omega_1 + 2\omega_2$) or 148 Hz($\omega_1 - 2\omega_2$).

The multiplier phototube detector signal current was dropped across a 16.2 K Ω load resistor to provide an input signal voltage to the phase-lock amplifier. The value of the load resistor was chosen to yield the lowest noise in the system compatible with reasonable input voltages for the range of signal current expected. With this load resistor, phototube signals of between 10^{-5} and 10^{-9} amperes yielded voltages of between 160 millivolts and 16 microvolts which nearly spanned the input signal range of the phase-lock amplifier.

The output of the phase-lock amplifier was 1 volt full scale for the sensitivity range in use. A voltage divider was constructed to permit a signal one-hundredth of the output to be used to drive a 10 millivolt recorder full scale.

Solutions

Solutions of each element to be analyzed were prepared from reagent grade chemicals. Stock solutions for Ag, Ca, Cd, Cr, Cu, Fe, Mg and Ni were made from AgNO_3 , $\text{Ca}(\text{C}_2\text{H}_3\text{O}_2)_2 \cdot \text{H}_2\text{O}$, $\text{CdCl}_2 \cdot 2\frac{1}{2}\text{H}_2\text{O}$, $\text{K}_2\text{Cr}_2\text{O}_7$, $\text{CuSO}_4 \cdot 5\text{H}_2\text{O}$, $\text{FeSO}_4 \cdot 7\text{H}_2\text{O}$, MgSO_4 , $\text{Mg}(\text{ClO}_4)_2$ and $\text{NiSO}_4 \cdot 6\text{H}_2\text{O}$, respectively. Three solutions of relative concentration 1.00, 0.50 and 0.25 were prepared for each decade of concentration examined. All solutions were prepared as aqueous solutions using high

quality deionized water except for the $\text{Mg}(\text{ClO}_4)_2$ solutions which were prepared in absolute ethanol.

Experimental Procedure

The practical analytical operating conditions for the system were either the manufacturer's recommended conditions or were experimentally chosen to give the optimum signal. The source was run at 12 amperes and 12.5 volts dc. The spectral bandwidth, s , and the spectral modulation amplitude, a , were maintained at a ratio of 1. The actual spectral bandwidth used in the experiments varied between 0.3 \AA and 0.5 \AA . The slit height was kept at 2 mm. Due to the variation in source intensity from wavelengths around 4000 \AA to 2300 \AA , the sensitivity setting of the phase-lock amplifier was adjusted to a level compatible with acquiring the phototube signal without overloading either the input or output amplifiers. The time constant employed in most experiments was 300 milliseconds although for very small signals a 1 second time constant was employed. The phase setting of the phase-lock amplifier was adjusted at the beginning of each experiment to yield the maximum signal. Data were taken with the monochromator in the non-scanning mode. The wavelength was set manually to give the maximum signal deflection on the recorder. Thermal drift of the monochromator away from the preset wavelength did not prove

to be a problem and an entire set of data could be collected without the necessity for readjustment of the monochromator. A nearly stoichiometric flame was used for all analyses except for Ca and Cr for which a fuel-rich flame was used. The acetylene-air flame supported on the 3-slot burner was very "soft" and had a marked tendency to waver about the optical axis due to drafts of air in the laboratory. This condition was remedied by placing sheets of aluminum behind and in front of the flame extending from the bench top nearly to the exhaust hood.

CHAPTER IV

RESULTS AND DISCUSSION

Verification of Theory

Various experiments were performed to test the validity of the theoretical expressions derived in Chapter II. The results of these are discussed below and summarized in Table 4.

Optimum Slit Width to Modulation Amplitude Ratio

The experiment to determine the optimum spectral bandwidth-to-spectral modulation amplitude ratio to verify Balslev's prediction [13] involved using a set of fixed straight slits of spectral bandwidth 0.40 \AA . The signal resulting from the aspiration of a solution of $10 \mu\text{g ml}^{-1}$ Ca into the flame was measured as a function of spectral modulation amplitude. The results are plotted in Figure 10. It may be seen that the theoretical optimum and the experimental optimum agree within about 3 per cent which is within experimental error.

First Derivative Mode Versus Second Derivative Mode

Equation (36) predicts that when the spectral modulation interval is equal to the spectral bandwidth, the

TABLE 4

VERIFICATION OF THEORY

Experiment	Conditions	Predicted Results	Experimental Results
Signal vs Spectral Modulation Amplitude at Constant Slit Width	10 $\mu\text{g ml}^{-1}$ Ca aspirated. 25 μ slit = 0.40 \AA	Maximum signal at 0.40 \AA (a)	Maximum signal at 0.41 \AA
Comparison of Magnitudes of 1st and 2nd Derivative Signals	Conditions identical for both. 10 $\mu\text{g ml}^{-1}$ Ca aspirated. Spectral modulation interval equal to spectral bandwidth	Ratio of $\frac{1st}{2nd} = 1.7$ (b)	Ratio of $\frac{1st}{2nd} = 1.4$
Comparison of Normal AAC with 1st Derivative AAC	25 $\mu\text{g ml}^{-1}$ Ca aspirated. All instrumental parameters identical for both cases.	Normal AA Signal 7.7 mv. (c) Derivative Signal 3.3 mv. (d)	Normal AA Signal 15.6 mv. Derivative Signal 3.3 mv.

Table 4 (Cont'd)

Experiment	Conditions	Predicted Results	Experimental Results
Verification of Photon Noise Limitation	1 $\mu\text{g ml}^{-1}$ Ca aspirated. Xenon arc vs tungsten-halogen lamp	$\frac{(S/N)_1}{(S/N)_2} = 0.3$ (e)	$\frac{(S/N)_1}{(S/N)_2} = 0.5$
Detection at Sum and Difference Frequencies for 1st Derivative	5.0 $\mu\text{g ml}^{-1}$, 1.0 $\mu\text{g ml}^{-1}$ and 0.5 $\mu\text{g ml}^{-1}$ Cu measured at 313 Hz and 203 Hz	Sum = Difference (f)	5.0 $\mu\text{g ml}^{-1}$ Sum = 1872 μV ; Difference = 1916 μV . 1.0 $\mu\text{g ml}^{-1}$ Sum = 420 μV ; Difference = 420 μV . 0.5 $\mu\text{g ml}^{-1}$ Sum = 225 μV ; Difference = 213 μV .

^aSee page 30 Chapter II.

^bSee Equation (36).

^cSee Reference [20].

^dSee Equation (34).

^eSee Equation (48).

^fSee Equation (32).

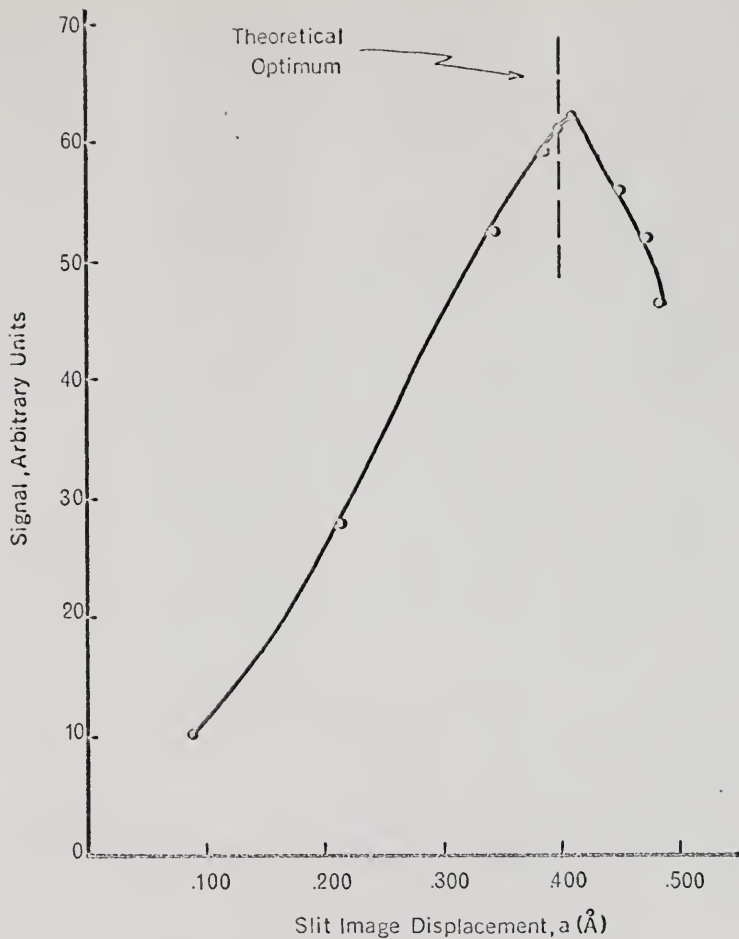


Fig. 10.---First derivative signal intensity versus spectral modulation amplitude (slit image displacement) at constant spectral bandwidth of 0.40 \AA .

ratio of the magnitudes of the first and second derivative signals is equal to 1.7. An experiment was performed at three different slit widths but at the same a/s ratio of unity. The mean ratio was found experimentally to be 1.4.

Normal AAC Compared with Derivative AAC

Comparisons of different analytical techniques are usually not valid since one experimentalist may compare results obtained with his system to those obtained in another laboratory under different conditions with different instrumentation in many cases. The only way to obtain a truly fair comparison is to perform both analytical techniques under the same laboratory conditions using as many common pieces of instrumentation as possible. In this manner, differences which arise may be attributed to the differences in technique. To this end, both normal atomic absorption spectrometry using a continuum source (AAC) and derivative AAC were performed using the same instrumentation. All experimental conditions, slit width and height, source power, flame conditions and analyte concentrations were identical for both techniques. The only difference between the techniques was oscillation of the refractor plate in the derivative technique.

The signals predicted by theory for normal AAC [20] and for the first derivative signal by Equation (34) for $25 \mu\text{g ml}^{-1}$ of Ca were calculated and compared with experi-

mental values. The results are listed in Table 4 and are in good agreement. Furthermore, even though the signal magnitude for normal AAC was five times larger than for the first derivative AAC signal, the S/N ratio was about five times poorer.

Direct comparison of results obtained with the present system with the best previous results by normal AAC [5] were unfavorable to the derivative system. However, the systems were different enough that the arguments raised in the first paragraph apply. When comparison was made on equal terms, that is, using ethanolic solutions of analyte and the same instrumentation, the derivative system proved to have an advantage in S/N ratio.

Photon Noise Limitation

All signal-to-noise and minimum detectable concentration expressions derived above have been predicated on the assumption that photon noise is the limiting noise in the present system. Equation (44) predicts that for all other parameters being constant, S/N should vary as the square root of the source radiance, $B_{\lambda_0}^0$. By using two sources the ratio of whose radiances is known, one can verify the prediction of Equation (44). Writing Equation (44) for the two sources and taking the ratio results in the following expression

$$\frac{(S/N)_1}{(S/N)_2} = \left[\frac{W_1 H_1 (B_{\lambda_0}^o)_1 s_1}{W_2 H_2 (B_{\lambda_0}^o)_2 s_2} \right]^{1/2} \quad (48)$$

Experimentally, a tungsten-iodine lamp and xenon arc were used as the sources and had a radiancy ratio of 0.16 at the wavelength of measurement, 4227 Å. A 1 µg ml⁻¹ solution of Ca was used as the experimental probe. The ratio calculated from the appropriate experimental parameters was 0.3 while the experimentally determined ratio was found to be 0.5.

Frequency of Detection

Equation (32) predicts that the first derivative signal should appear at both the sum and difference frequencies. An experiment measuring three concentrations of Cu (5.0 µg ml⁻¹, 1.0 µg ml⁻¹ and 0.5 µg ml⁻¹) was carried out at the sum and difference frequencies. The results are tabulated in Table 4 and are in close agreement.

Analytical Curves and Limits of Detection

Analytical curves were constructed from measurements made with the system in the first derivative mode for Ag, Ca, Cd, Cr, Cu, Fe, Mg, and Ni and are illustrated in Figures 11 through 18, respectively. The analytical lines employed, the type of transition which occurred [27], degree of atomization [28], statistical weight of the state

Fig. 11.--Analytical curve for silver taken at 3280 Å.

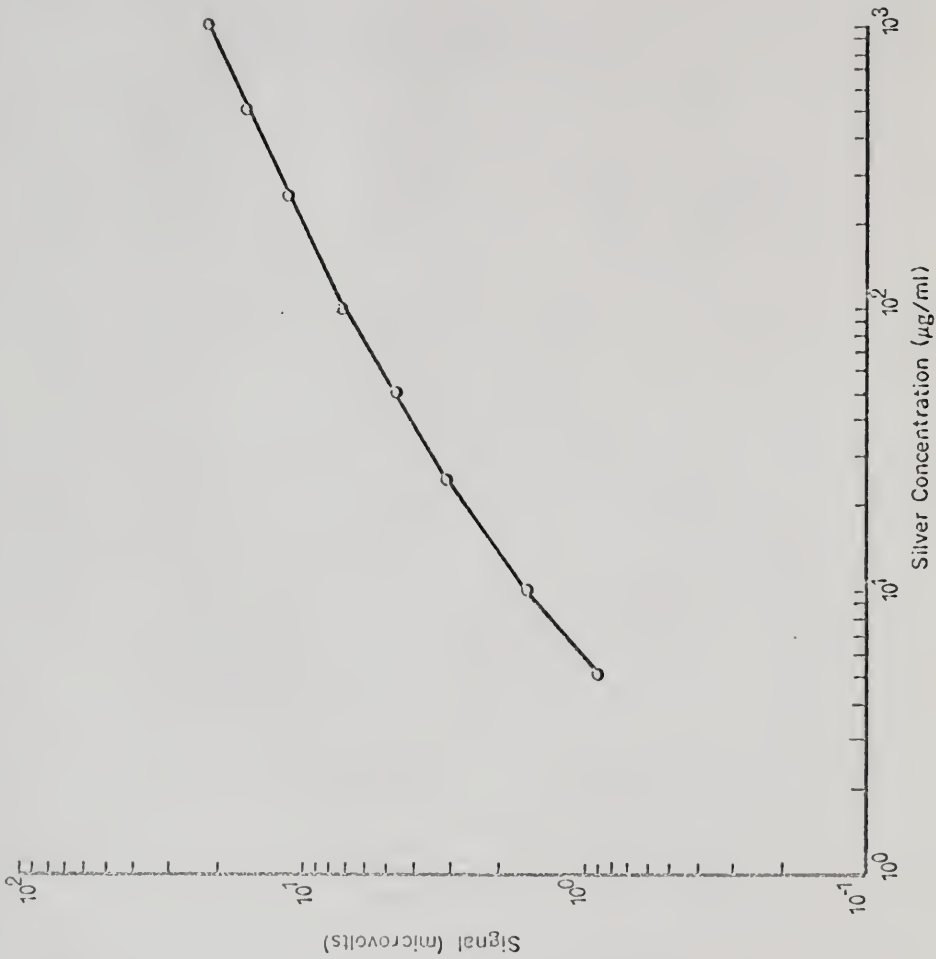


Fig. 12.--Analytical curve for calcium taken at 4227 Å.

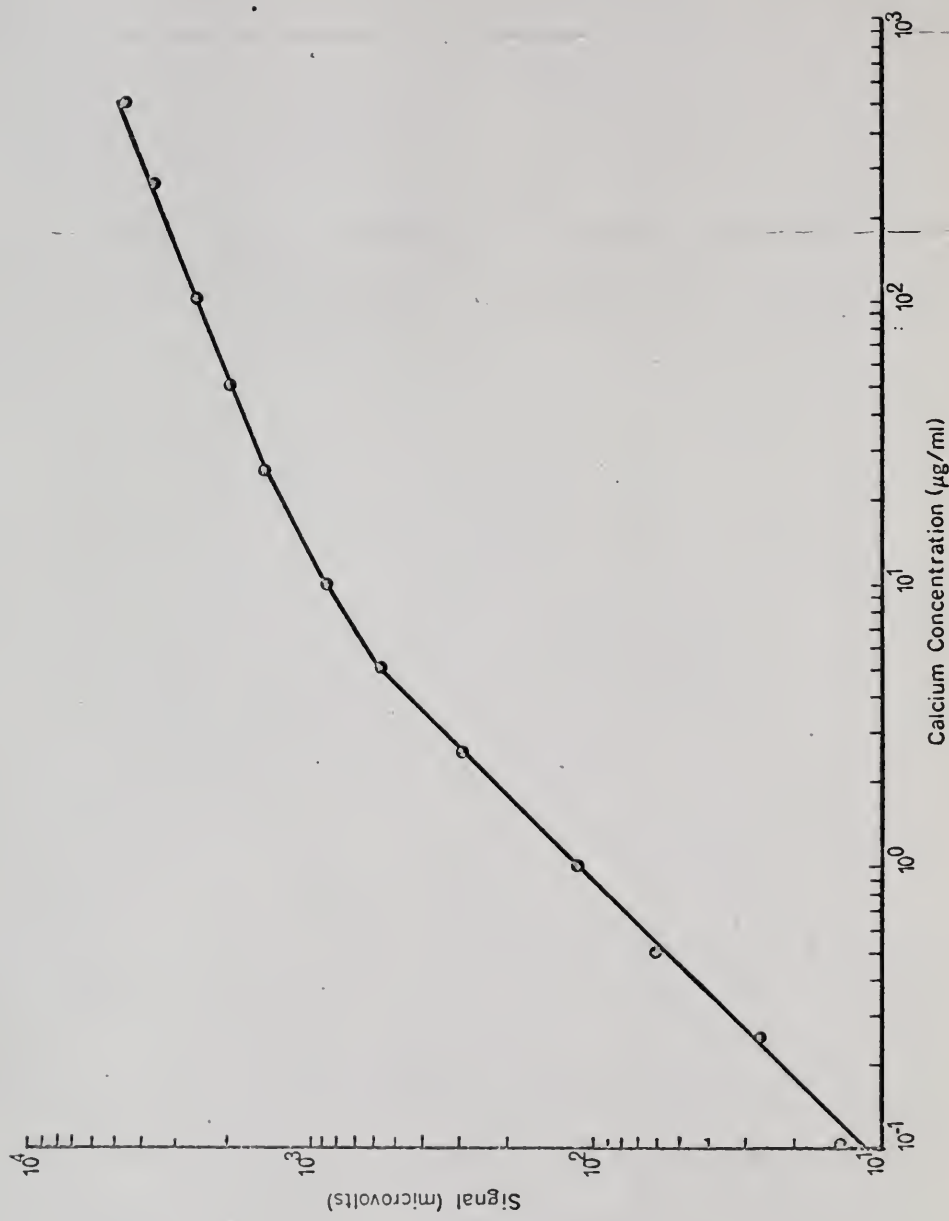


Fig. 13.--Analytical curve for cadmium taken at 2288 Å.

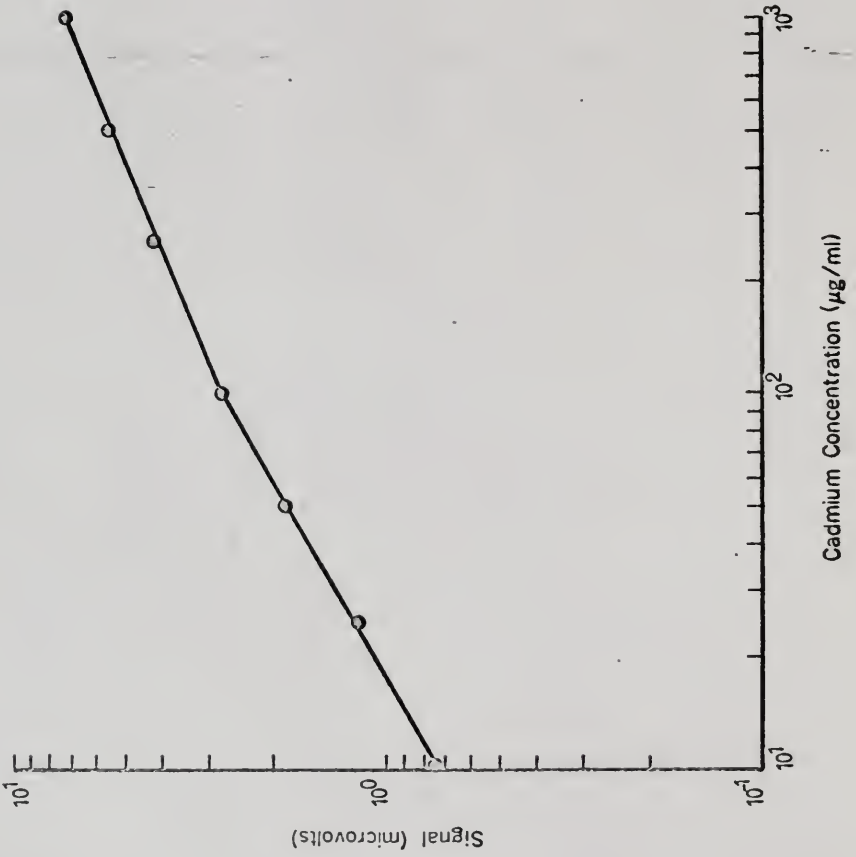


Fig. 14.--Analytical curve for chromium taken at 3579 Å.

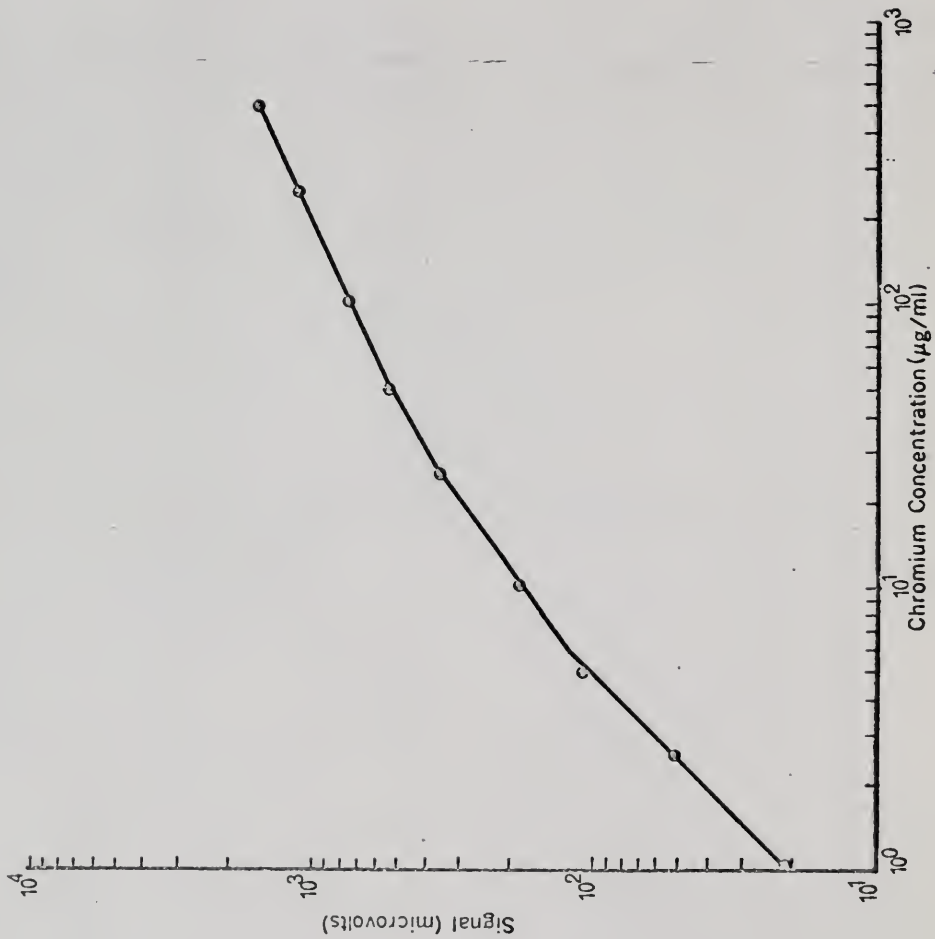


Fig. 15.---Analytical curve for copper taken at 3247 Å.

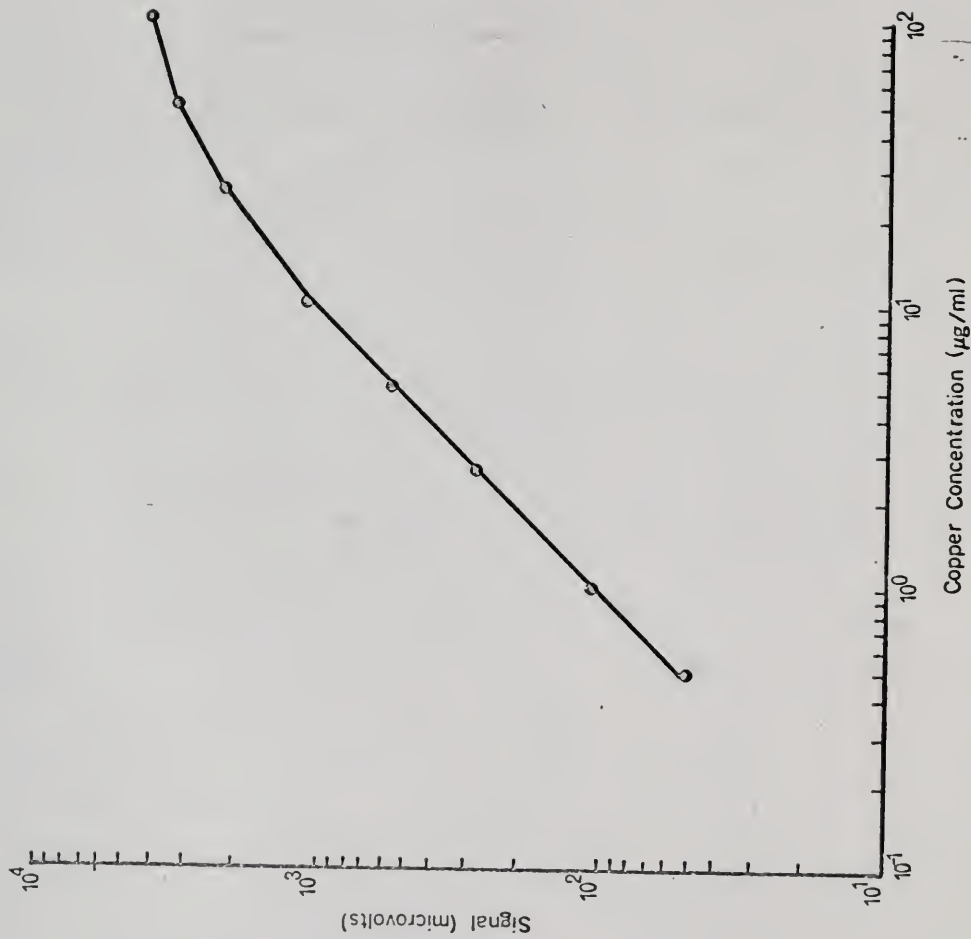


Fig. 16.--Analytical curve for iron taken at 3719 Å.

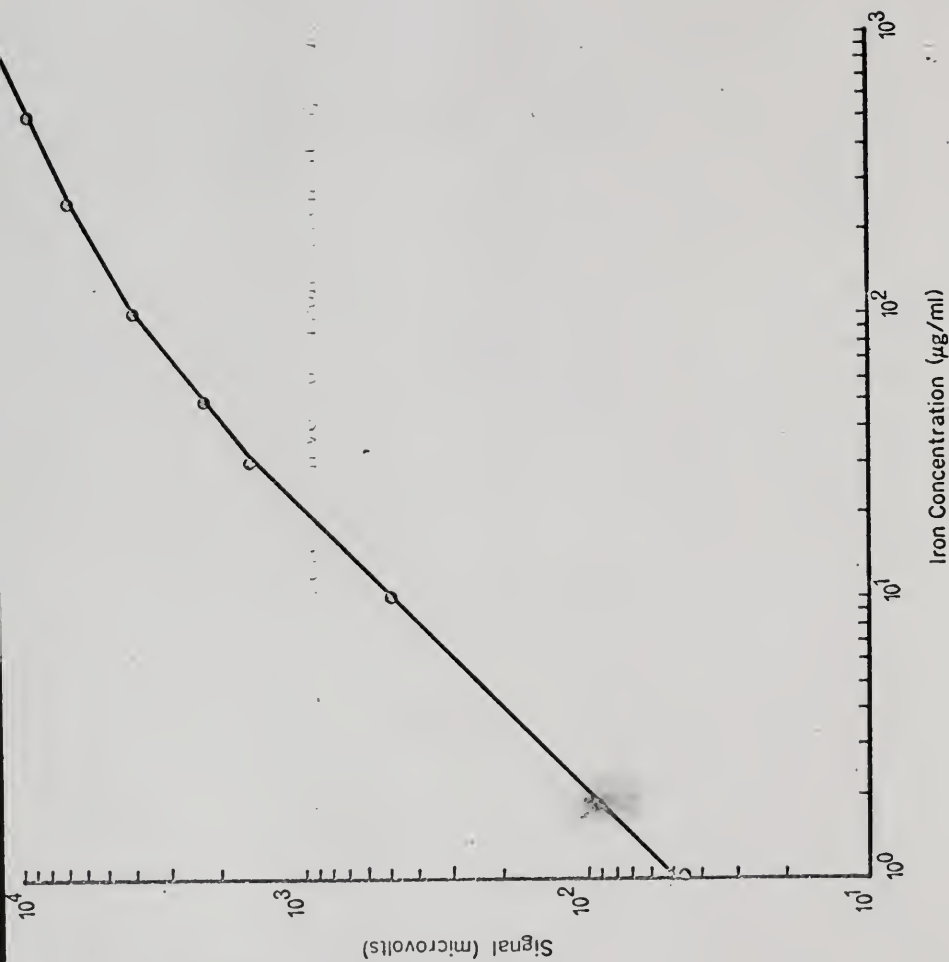


Fig. 17.--Analytical curve for magnesium taken at 2852 Å.

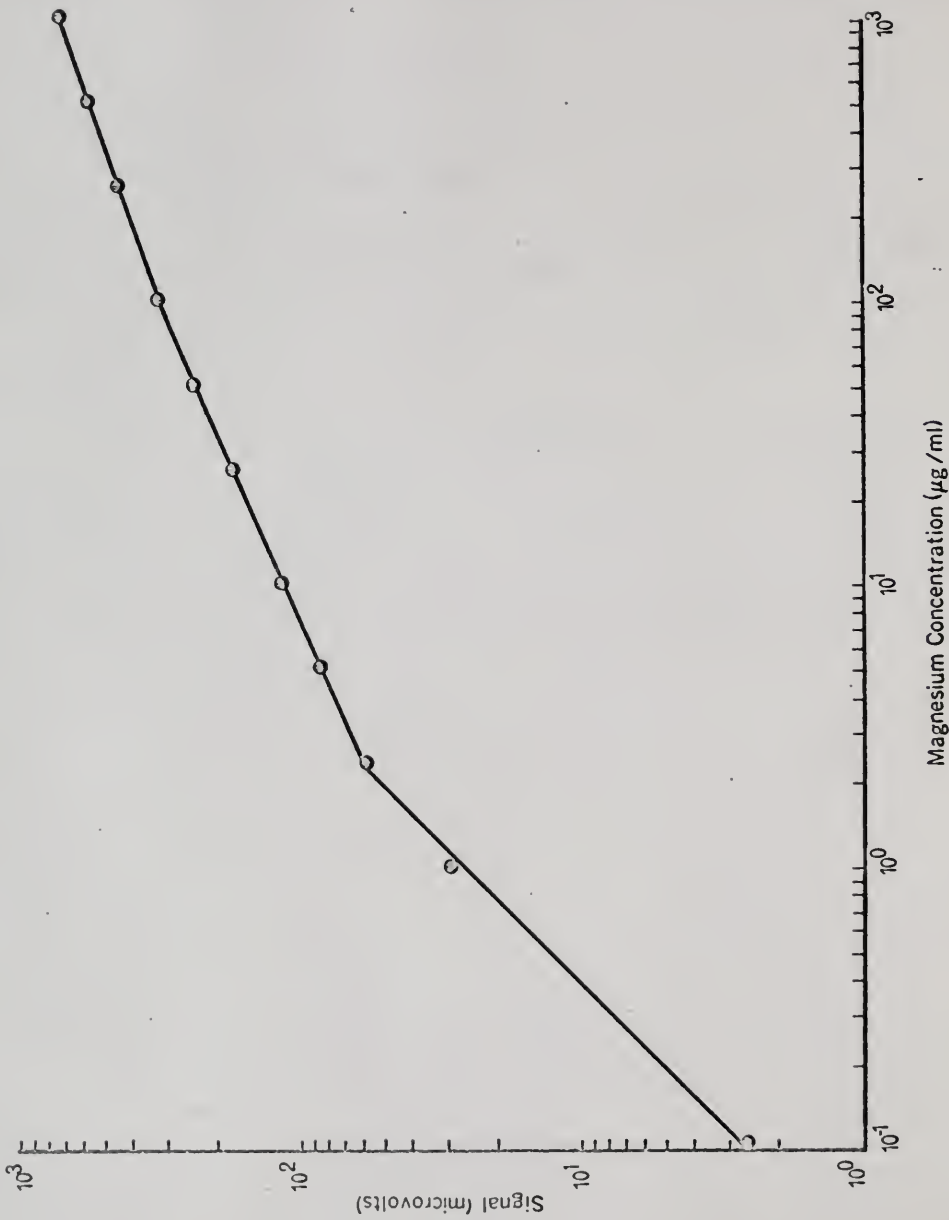


Fig. 18.---Analytical curve for nickel taken at 3414 Å.

from which absorption occurred [27], the oscillator strength for the transition [27], the electronic partition function [29], the theoretical limits of detection calculated using Equation (43) and the experimental limits of detection are tabulated in Table 5. Experimental limits of detection were obtained by extrapolating the analytical curves to the point where the signal was equal to twice the rms noise and reading the corresponding concentration.

Because the derivative spectrometer is sensitive to small, but rapid, changes in the slope of the spectrum it views, both the source and flame background spectra were examined over an interval of 5 \AA on either side of the analytical lines used. In all cases, the source background varied linearly and had no fine structure in its spectrum. In the cases of Mg, Cr, and Fe, there were some flame emission lines within the 10 \AA interval, but these were far enough away from the analytical lines not to interfere.

It should be noted that the general shape of all analytical curves follows that of the theoretical curve of growth in Figure 3 having a slope of 1 at low concentrations and a slope of less than 1 at concentrations greater than $10 \mu\text{g ml}^{-1}$ which corresponds approximately to an atomic concentration in the flame of $10^{10} \text{ atoms cm}^{-3}$.

TABLE 5

LIMITS OF DETECTION

Element	Analytical Line (Å)	Atomic Transition [27]	β [28]	B(T) [29]	gf [27]	gi [27]	f [27]	Theoretical C_m $\mu\text{g ml}^{-1}$	Actual C_m $\mu\text{g ml}^{-1}$
Cadmium	2288	$1S_0-1P_1$	0.38	1	0.92	1	0.92	5	10
Magnesium	2852	$1S_0-1P_1$	1.06	1	1.1	1	1.1	2×10^{-2}	10^{-1}
Copper	3247	$2S_{1/2}-2P_{3/2}$	0.88	2	.64	2	.32	7×10^{-2}	5×10^{-1}
Silver	3280	$2S_{1/2}-2P_{3/2}$	0.70	2	.53	2	.27	2×10^{-1}	2
Nickel	3414	$3D_3-3D_3^0$	-	25	1.0	7	.14	-	2
Chromium	3579	$7S_3-7P_4$.071	7	1.6	7	.23	4×10^{-1}	4×10^{-1}
Iron	3719	$5D_4-5F_5$	0.84	18	.52	9	.06	2×10^{-1}	4×10^{-1}
Calcium	4227	$1S_0-1P_1$.07	1	.28	1	.28	1×10^{-1}	1×10^{-1}

Conclusions

The advantages of using a continuum source in atomic absorption spectrometry versus line sources have been enumerated earlier. In addition to the cost and time saving advantages, one further important capability is present. When using line sources, the analyst is restricted to utilizing resonance transitions, that is, transitions arising from the ground state, since these are usually the most strongly emitted lines of the source. However, in certain cases, for example, Ni, and Fe, there are very low lying states having large transition probabilities which may be appreciably populated at the temperature of the flame. Systems employing continuum sources may take advantage of these more favorable transitions while those using line sources generally may not.

It is shown in Table 4 that the signal obtained for identical concentrations of analyte was larger for normal mode AAC than for the first derivative mode by a factor of about 5. Why, then, use the derivative mode in favor of the normal mode? The answer is that the signal-to-noise ratio of the derivative mode is 5 times that of the normal mode. In addition, if the absorption peak happens to be superimposed on a slowly increasing or decreasing background, no background baseline correction need be applied since the first derivative of such a slope is a constant.

The advantage of using double modulation over just wavelength modulation as in Snelleman's system [17] is that all of the signal arising from the flame due to emission is totally rejected. In addition, the use of a piezoelectric transducer to drive the refractor plate simplifies the system to the extent that no major modifications need to be made to the monochromator as in other systems employing rotating mirrors or refractor plates or vibrating slits. All that is required to revert to the normal mode is to stop the oscillation of the refractor plate.

An additional capability of the system allows first or second derivative operation in the emission mode, as in Snelleman et al. [16], by simply turning off the source and chopper and detecting at ω_2 or $2\omega_2$ for the first or second derivative signal, respectively.

The chief limitation of the present system is that the radiancy of the source is insufficient to push the minimum detectable concentration into the 10^{-3} to 10^{-2} $\mu\text{g ml}^{-1}$ range where it could compete more favorably with line source atomic absorption spectrometry.

Several possibilities to improve the system suggest themselves. The first is to utilize a source of considerably greater radiancy between 2300 Å and 4200 Å. The second is to improve the transmission of light through the system. The latter could be accomplished by using mirrors instead of quartz lenses. A third would be to substitute

a non-flame cell such as a graphite filament for the flame. By incorporating these improvements into the present system, the minimum detectable concentration should be lowered considerably, for example, by at least one order of magnitude.

However, even with these limitations, the present system is sensitive enough to be recommended as a useful, convenient analytical tool in areas such as the steel industry or agricultural industry where sample size is not highly important. If the above improvements can be realized, the system may also find important use in clinical and bioanalytical applications.

LIST OF REFERENCES

1. A. Walsh, *Spectrochim. Acta* 7, 108-117(1955).
2. W.W. McGee and J.D. Winefordner, *Anal. Chim. Acta* 37, 429-435(1967).
3. L. de Galan, W.W. McGee and J.D. Winefordner, *Anal. Chim. Acta* 37, 436-444(1967).
4. J.D. Winefordner, V. Svoboda and L.J. Cline, *CRC Critical Reviews in Analytical Chemistry* 1, 233-274 (1970).
5. V.A. Fassel, V.G. Mossotti, W.E.L. Grossman and R.N. Knisely, *Spectrochim. Acta* 22, 347-357(1966).
6. J.H. Gibson, W.E.L. Grossman and W.O. Cooke, *Proc. Feigl Anniv. Symp.*, 287-290(1962).
7. A.T. Giese and C. Stacy French, *Appl. Spectros.* 9, 78-94(1955).
8. G.L. Collier and F. Singleton, *J. Appl. Chem.* 6, 495-510(1956).
9. G. Bonfiglioli and P. Brovetto, *Appl. Optics* 3, 1417-1424(1964).
10. A. Perregaux, and G. Ascarelli, *Appl. Optics* 7, 2031-2035(1968).
11. G. Bonfiglioli, P. Brovetto, G. Busca, S. Leviaidi, G. Palmieri and E. Wanke, *Appl. Optics* 6, 447-455(1967).
12. F.R. Stauffer and H. Sakai, *Appl. Optics* 7, 61-65(1968).
13. I. Balslev, *Phys. Rev.* 143, 636-647(1966).
14. D.T. Williams and R.N. Hager, Jr., *Appl. Optics* 9, 1597-1605(1970).
15. K.L. Shaklee and J.E. Rowe, *Appl. Optics* 9, 627-632 (1970).

16. W. Snelleman, T.C. Rains, K.W. Yee, H.D. Cook and O. Menis, *Anal. Chem.* 42, 394-398(1970).
17. W. Snelleman, *Spectrochim. Acta* 23B, 403-411(1968).
18. F. Aramu and A. Rucci, *Rev. Sci. Inst.* 37, 1696-1698 (1966).
19. R.N. Hager, Jr., and R.C. Anderson, *J. Opt. Soc. Am.* 60, 1444-1449(1970).
20. J.D. Winefordner and T.J. Vickers, *Anal. Chem.* 36, 1947-1954(1964).
21. A.C.G. Mitchell and M.W. Zemansky, *Resonance Radiation and Excited Atoms*, 2nd ed., 1961, Cambridge University Press, New York, N. Y.
22. S.S. Penner, *Quantitative Molecular Spectroscopy and Gas Emissivities*, Addison-Wesley Publishing Co., 1959.
23. H.J. Kostkowski and A.M. Bass, *J. Opt. Soc. Am.* 46, 1060-1064(1956).
24. Yu. I. Belyaev, L.M. Ivantsov, A.V. Karyakin, Pham Hung Phi and V.V. Shemet, *Anal. Khim.* 23, 980-986(1968).
25. L.D. Landau and E.M. Lifshitz, *Theory of Elasticity*, Addison-Wesley Publishing Co., 1959.
26. Bulletin PD-9247, Gould Inc., Piezoelectric Division, 232 Forbes Road, Bedford, Ohio, 1969
27. R. Mavrodineanu and H. Boiteaux, *Flame Spectroscopy*, John Wiley and Sons, Inc., New York, N. Y., 1965.
28. L. de Galan and G.F. Samaey, *Spectrochim. Acta* 25B, 245-259(1970).
29. L. de Galan, R. Smith and J.D. Winefordner, *Spectrochim. Acta* 23B, 521-525(1968).


BIOGRAPHICAL SKETCH

Robert Cooper Elser was born September 13, 1941, at Mechanicsburg, Pennsylvania. In June, 1959, he was graduated from Mechanicsburg Area High School in Mechanicsburg, Pennsylvania. In June, 1963, he was graduated from Lehigh University, in Bethlehem, Pennsylvania, with a Bachelor of Science degree in Chemistry. While at Lehigh University, he was a member of Alpha Tau Omega social fraternity and Omicron Delta Kappa, a national men's leadership honorary fraternity. Upon graduation he became affiliated with the Allentown Hospital, in Allentown, Pennsylvania, as the assistant to the biochemist. In July, 1964, he accepted a position as supervisor of clinical chemistry laboratories at The Reading Hospital, in West Reading, Pennsylvania, and remained in that capacity until August, 1967, when he entered the Graduate School at the University of Florida in Gainesville, Florida. While at the University of Florida, he has held a National Institutes of Health Traineeship, a graduate research assistantship and a Graduate School Fellowship.


He is a member of the American Chemical Society and the American Association of Clinical Chemists.

Robert Cooper Elser is married to the former Kay Elizabeth Wolfe and has two sons, Christopher Wirt and Peter Richard.

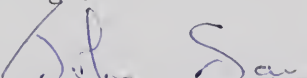
I certify that I have read this study and that in my opinion it conforms to acceptable standards of scholarly presentation and is fully adequate, in scope and quality, as a dissertation for the degree of Doctor of Philosophy.


James D. Winefordner, Chairman
Professor of Chemistry


I certify that I have read this study and that in my opinion it conforms to acceptable standards of scholarly presentation and is fully adequate, in scope and quality, as a dissertation for the degree of Doctor of Philosophy.


Roger G. Bates
Professor of Chemistry

I certify that I have read this study and that in my opinion it conforms to acceptable standards of scholarly presentation and is fully adequate, in scope and quality, as a dissertation for the degree of Doctor of Philosophy.


John Savory
Associate Professor of Pathology

I certify that I have read this study and that in my opinion it conforms to acceptable standards of scholarly presentation and is fully adequate, in scope and quality, as a dissertation for the degree of Doctor of Philosophy.


Gerhard H. Schmid
Associate Professor of Chemistry

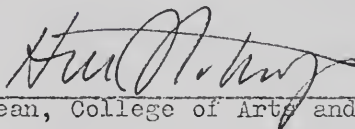
I certify that I have read this study and that in my opinion it conforms to acceptable standards of scholarly presentation and is fully adequate, in scope and quality, as a dissertation for the degree of Doctor of Philosophy.



Eugene Sander
Associate Professor of Biochemistry

This dissertation was submitted to the Dean of the College of Arts and Sciences and to the Graduate Council, and was accepted as partial fulfillment of the requirements for the degree of Doctor of Philosophy.

June, 1971



Dean, College of Arts and Sciences

Dean, Graduate School

#599 Lee Mun 68
(126)

GA 1.0. 13.189.